Alma Mater Studiorum · Università di Bologna

FACOLTÀ DI SCIENZE MATEMATICHE, FISICHE E NATURALI
Corso di Laurea Specialistica in Fisica

Dynamical aspects of optical acceleration and transport of protons

Tesi di Laurea in Meccanica Analitica

Relatore:
Chiar.mo Prof.
Giorgio Turchetti

Candidato:
Stefano Sinigardi

II Sessione
Anno Accademico 2009-2010

Sommario

Il lavoro di tesi, svolto nel gruppo V dell'INFN di Bologna, mi ha permesso di iniziare a conoscere un ambito di ricerca particolarmente attivo a livello internazionale. L'accelerazione di particelle con l'uso di laser è diventato di notevole interesse grazie al rapidissimo aumento di potenza che ha caratterizzato lo sviluppo dei laser nell'ultimo decennio.

L'accelerazione di elettroni ha già raggiunto un buon grado di comprensione teorica e di affidabilità sperimentale, grazie allo studio dei wake-fields. Le energie raggiunte sono dell'ordine dei GeV con apparecchi di dimensioni table-top e la qualità del fascio è tale che sono già allo studio sistemi multi-stage per acceleratori di particelle futuri.

Le tecniche di accelerazione laser-plasma sono invece ancora ampiamente sotto indagine per i protoni e gli ioni in generale. Solo recentemente si stanno iniziando ad avere risultati interessanti, con pacchetti di protoni di qualche MeV di energia. Grazie allo studio di nuovi bersagli gassosi, sembra possibile in un prossimo futuro ottenere protoni con energie dell'ordine del centinaio di MeV, sufficienti per avere interessanti applicazioni soprattutto in ambito medico con l'adroterapia.

Nel primo capitolo di questa tesi descrivo le principali tecniche di accelerazione di ioni indagate fino ad oggi e i risultati che stanno mostrando. Quindi, nel secondo capitolo, analizzo metodi di simulazione computazionale del comportamento di un plasma e di un fascio accelerato, partendo dallo studio di diversi tipi di integratori numerici delle equazioni differenziali che caratterizzano la meccanica del sistema, fino a giungere, nel terzo capitolo, alla modellizzazione degli elementi magnetici di una beamline che ne permetta il trasporto.

L'obiettivo è quello di iniziare la ricerca per l'ottimizzazione dei bersagli del laser, tramite l'identificazione di parametri minimi da soddisfare, e dei sistemi di trasporto, così che sia possibile un interfacciamento con apparecchi di post-accelerazione studiati da altri ricercatori

in contatto col nostro gruppo.

Per raggiungere questo obiettivo ho studiato diverse linee di trasporto, collaborando con il gruppo del Prof. Ratzinger dell'Università di Francoforte sul Meno (Germania) e con altri ricercatori del GSI di Darmstadt (Germania). I risultati sono ancora preliminari ma vengono qui presentati i più interessanti raggiunti durante il periodo di ricerca.

Introduction

In this thesis I will describe the work that I did with the 5^{th} group of INFN in Bologna. The research field they're working on is particularly active in Italy and in many other countries.

Particle acceleration through laser has become really attractive in the latest years mainly thanks to the great power enhances that the lasers experienced recently. Electron acceleration with laser is known relatively well: many articles describe the laser wake field and the ability of electrons to "surf" a magnetic wave to get energy. We already reach GeV energy with table-top devices and the beam quality is good enough that many multi-stage systems are under development for future electron accelerators.

On the other hand, laser-plasma acceleration techniques are still under heavy investigation for protons and ions in general. Only recently we're starting to get interesting results, obtaining some bunches with few-MeV protons. Now, thanks to gaseous jet targets, it seems that in the near future we will be able to get protons with energies in the hundredth of MeV, enough to have some interesting applications in medical treatments (hadron-therapy)

In this thesis I will describe, in the first chapter, the main techniques known up to date to accelerate ions with lasers and their results. In the second chapter I will analyse different kinds of numerical integration techniques through a software that I wrote. Those integrators are used to integrate the differential equations that describe the plasma motion and behaviour.

In the third chapter I will study the problems of transport of these bunches obtained from laser pulses. The goal is to optimize targets, through finding minimal necessary conditions required on the initial distributions, and to study transport systems required to collect as many protons as possible and bring them away from the interaction point. For the future,

we're also considering matching the laser accelerated protons with a second-stage accelerator and so we will need to design the best beamline.

To this aim, I studied and simulated with another software many different transport lines. I went also in Frankfurt am Main to work with Prof. Ratzinger's group, to check my software results and to investigate, with other people from GSI (Darmstadt), different solutions for this problem. In this thesis I will describe the best results that I got during this research period.

Contents

CHAPTER 1

Laser-Plasma accelerators

1.1 What is a plasma?

A plasma is a ionized gas. We should know about three states of matter: solid, liquid and gas. When a solid is heated enough, the thermal motion of the atoms breaks the lattice that builds the crystal and usually a liquid is formed. In the same way, a liquid heated over the boiling temperature has the property that its atoms vaporize faster than they re-condense.

Similarly, when a gas is heated sufficiently, collisions between atoms make them mislay their loosely bound electrons. The ions-electron mixture that we get is commonly called a plasma [1].

1.2 Particle acceleration

Particle acceleration is used as a way to answer profound questions about our universe. Giant machines accelerate those little fundamental elements of the matter to nearly the speed of light and then smash them together. In this way, it's possible to recreate conditions that existed when our universe was born in the big bang and unleash all the possible particles and interactions that exist, to understand how they are all connected, described and, maybe, unified in a single theory.

Unfortunately, to achieve always greater energies, we have to build bigger and more

expensive particle accelerators. The most powerful one at the moment is the LHC, made by CERN in Geneva[1]. It has reached every possible limit of what is technologically and economically feasible. Will advances in the science and engineering of particle accelerators be continuous so that we can have something else after LHC?

A new approach to particle acceleration, using the plasma state of matter, is showing considerable promise for realizing a new type of accelerators, dramatically reducing their size and cost.

This is only one part of the story: particle acceleration is also really important for material science, structural biology, fusion research, transmutation of nuclear waste and nuclear medicine, such as treatment of certain types of cancer, among others. Of course, in these cases, smaller ordinary machines are used now, but they still occupy large laboratory spaces. Plasma accelerators promise extremely compact devices even in this smaller energy range [2].

1.2.1 Accelerator basics

Accelerators propel either lighter particles (such as electrons and their antiparticle, positrons) or also heavier ones (protons, anti-protons and ions).

They can boost particles in a single passage (linear accelerators) or in many orbits (circular ring accelerators). A big problem of non linear acceleration is a process called synchrotron radiation. As we will see, linear acceleration (preferably of electrons and positrons) is what plasma based accelerators are most suited for.

A conventional linear collider accelerates its particles with an electric field that moves along in synchrony with the particles. A structure called a slow-wave cavity (a metallic pipe with periodically placed irises) generates the electric field using powerful microwave radiation. The use of a metallic structure limits how large the accelerating field can be. At a field of 20-50 MV/m, electrical breakdown occurs — sparks jump and current discharges from the walls of the cavities.

Because the electric field has to be weaker than the threshold for breakdown, it takes a longer acceleration path to achieve a specific energy. For example, a TeV beam would require an accelerator 30 kilometers long. If we could accelerate particles far more quickly than is allowed by the electrical breakdown limit, the accelerator could be made more compact. That is where plasma comes in.

[1] `http://lhc.web.cern.ch/lhc/` contains a lot of info about the Large Hadron Collider and its scientific program.

1.3 Lasers

In the last twenty years, the maximum power of the lasers has increased many order of magnitude, reaching intensities over 10^{21} W/cm^2. The field, at these values, reaches 10^{12} V/m, so it's greater than the electric field that binds electrons to the nucleus.

Electrons knocked by these intense electromagnetic pulses oscillate at relativistic speeds, with pulses up to 10 MeV/c. Radiation pressure made by laser is extreme and easily reaches terabars: we will describe it in the next chapter 1.5.

When a so strong pulse interacts with matter, it instantly ionizes everything, creating a plasma.

1.3.1 Chirped Pulse Amplification

The power increased so much in these years thanks to the Chirped Pulse Amplification (CPA) technique [3]. The fundamental idea is to use three devices: a "stretcher" and a "compressor", with an amplification crystal. We use a first pulse, made by a low power laser (oscillator) which is able to create a really short packet, $\sim$ 10 fs, then we "stretch" it to $\sim$ 10 ns. Then the pulse is amplified by the crystal, pumped by another laser, to get an amplification of 10 order of magnitude (so that we get an energy of a Joule). The pulse is then "compressed" back to the oscillator length.

The transverse dimensions of these pulses are approximately between some centimeters up to a meter. The reason is that the great electric fields intensities would ionize the air and could destroy everything. We have to focus them using a parabolic mirror to get peaks of 10^{21} W/cm^2 [4].

1.4 Plasma physics

1.4.1 Plasma accelerators

In a plasma accelerator, the role of the accelerating structure is played by the plasma. Instead of being a problem, electrical breakdown is part of the design because the gas is already broken down at the beginning. There's virtually no theoretical limit to the field that can be produced in a plasma, as long as quantum effects don't need to be considered. The power source is not microwave radiation but is either a laser beam or a charged particle beam.

At first sight, laser beams and charged particle beams do not seem well suited for particle acceleration. They can have very strong electric fields, but the fields are mostly perpendicular to the direction of propagation. To be effective, the electric field in an accelerator has

to point in the direction that the particle travels. Such a field is called a longitudinal field. Fortunately, when a laser or charged particle beam is sent through a plasma, interaction with the plasma can create a longitudinal electric field.

The process works in this way: a plasma as a whole is electrically neutral, containing equal amounts of negative charge (electrons) and positive charge (ions). A pulse from an intense laser or particle beam, however, creates a perturbation of the plasma density. In essence, the beam, via the so called *ponderomotive force* (see chapter 1.5), pushes the particles away from the high intensity regions. Being the ions much heavier than the electrons, they remain nearly unperturbed and a charge separation is created, accompanied by strong electrostatic fields. This perturbation induces a plasma wave that travels in the wake-field at the speed of the group velocity of the pulse itself. Those powerful electric fields, so, will accelerate any charged particles that come under their influence.

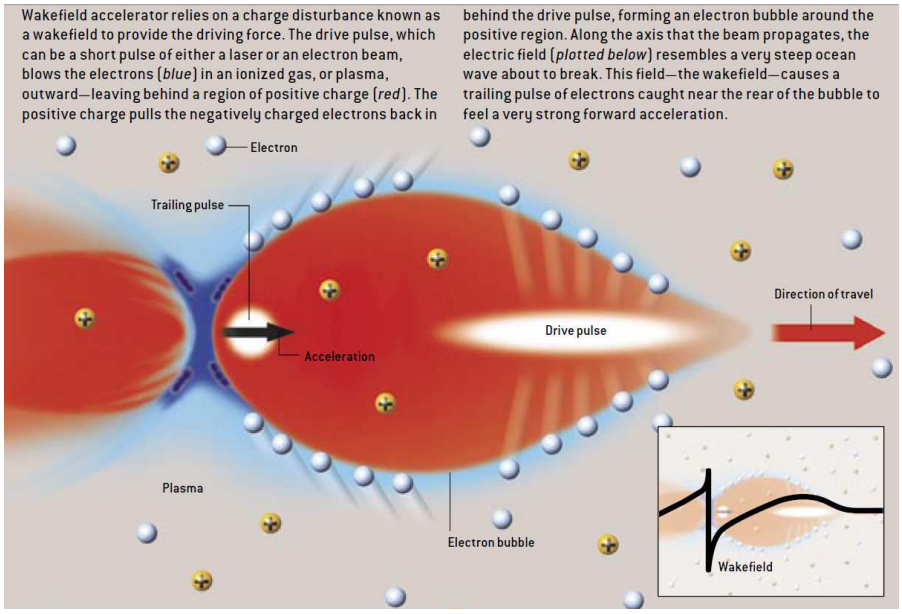

Figure 1.1: *The wakefield accelerator [2]*

A plasma medium can support accelerating electric fields of fantastic magnitude. A plasma containing 10^{18} electrons per cubic centimeter (an unexceptional number) can generate a wave with a peak electric field of 100 GV/m. That is more than 1000 times greater than the accelerating gradient in a typical conventional accelerator powered by microwaves. Now the catch: the wavelength of a plasma wave is only some μm, whereas the typical microwave wavelength is 10 cm. It is very tricky to place a bunch of electrons in such a microscopic wave, if we want to inject it. It works better if we try to self-break the wave, so that electrons come from the plasma itself.

Table-top-plasma accelerators are made possible today by intense, compact lasers. Ti:Sa

lasers that can generate 10 TW of power in ultra-short light pulses now fit on a large tabletop [5]. In a laser-powered plasma accelerator, for example, an ultra-short laser pulse is focused into a helium supersonic gas jet that can be some millimeters long. The pulse immediately strips off the electrons in the gas, producing a plasma. The radiation pressure of the laser bullet is so great that the much lighter electrons are blown outward in all directions, leaving behind a positively charged region. These electrons cannot go very far, because the electric field generated by the charge displacement pulls them back. When they reach the axis the laser pulse is traveling along, another pulse overshoots them and they end up traveling outward again, producing a wavelike oscillation [Figure 1.1]. The oscillation is called a laser wake-field because it trails the laser pulse like the wake produced by a motorboat.

Unfortunately, the accelerated electrons had a very wide range of energies — from 1 to 200 MeV. Many applications require a beam of electrons that are all at the same energy. This energy spreading occurred because the electrons were trapped by the wake-field wave at various locations and at different times. In a conventional accelerator, particles to be accelerated are injected into a single location near the peak of the electric field. Researchers thought that such precise injection was impossible in a laser wake-field accelerator because the accelerating structure is microscopic and short-lived.

The accelerated electron bunch can be externally injected, using a conventional accelerator, another laser-plasma stage or "internally" injected. This kind of injection comes from the so called wavebreaking of the plasma wave generated in the trail of the laser pulse. In particular conditions, the electron front at the peak density in the wake of the laser pulse can break like a wave in the sea. When some of the electrons of the wave have a speed higher than the wave velocity they leave the collective motion and find themselves injected in front of the wave (a kind of foam, speaking in sea-terms!). An injected electron bunch experiences the strong accelerating electric field previously described and travels in the wake of the laser pulse gaining high energies. The most easily obtained wavebreaking comes spontaneously when the density perturbation is very high.

Many techniques are already used or under development and they ensure a high monochromaticity of the electron bunches generated by a plasma accelerator and a small emittance. These techniques aim to induce the wave breaking in more controlled ways, for example using a non uniform gas jet (the plasma wave speed depends on the plasma density), or using a second weak counter-propagating laser which perturbs for a short time the plasma wave.

This small energy spread and the small emittance of the produced electron bunches, together with their very short time duration, might allow the development of multi-staged plasma accelerators in the near future.

The laser-plasma interaction, using different experimental setups, can also be used to accelerate heavier ions. Unfortunately, many of these techniques require that the injected protons/ions must be already traveling at nearly the speed of light, so they are not left behind by the plasma wave. For protons, that means an injection energy of several GeV.

Other alternatives, described in this thesis, use the strong electric fields that the charge displacement creates to accelerate ions (protons) up to some MeV. The protons/ions come from the target itself, often from a hydrogen-rich layer placed above it.

Physicists are making rapid progress in the quest for a plasma accelerator. Although many of the fundamental physics issues are solved, the making of practical devices still poses formidable challenges. In particular, beam engineers must achieve adequate beam quality, efficiency (how much of the driver beam's energy ends up in the accelerated particles), and alignment tolerances (the beams must be aligned to sub μm at the collision point). Finally, the repetition rate of the device (how many pulses can be accelerated each second) is important.

It took conventional accelerator builders 75 years to reach electron-positron collision energies in the range of 200 GeV. Plasma accelerators are progressing at a faster rate, and researchers hope to provide the new technology to go beyond the microwave systems for high-energy physics in just a decade or two. Much sooner than that, the companion laser wake-field technology will result in GeV tabletop accelerators for a rich variety of applications [6].

1.4.2 Characteristics of plasma

Plasma is pervasive in nature: surfaces of stars, interstellar gases, Terrestrial magnetosphere, these are all examples of plasmas.

The science of plasma physics was developed both to understand these natural phenomena and to explore the realm of controlled nuclear fusion.

What are the characteristics of plasmas? The important point is that the dynamics of motion are determined only by forces between near atoms of the material: the range of the forces in such a configuration is limited.

Let's start with a system of N charges, which are coupled one to another via their self-consistent electric and magnetic fields. If we need to consider each and every aspect of those charges, we would have 6N coupled equations.

Fortunately, a very great simplification is possible if we focus our attention to collisionless plasma: in this case, we can decompose the electric field in two parts. $\mathbf{E}_1$ has a space variation on a scale thinner than the *Debye length*, which is the length over which the field of an individual charge is shielded out by the surrounding particles, and represents the rapidly fluctuating microfield. $\mathbf{E}_2$, on the other hand, represents the field due to deviations from charge neutrality over space scales greater than the Debye length [7].

1.4.3 Debye length

Let's consider a uniform charge distribution, electrons for example, with density n_0. In a neutral plasma, we will have an equal distribution of ions, so that the system is neutral. Let's suppose that some electrons get moved so that their density becomes $n \neq n_0$, in a way that we could write $n = n_0 + n_1$. The basic hypothesis that we do is that the new distribution is in thermal equilibrium at a temperature T. Under these conditions, denoting the potential generated by the n distribution with V, we have

$$n = n_0 \exp(eV/k_B T)$$

where, as obvious, e is the electron charge. Defining with $\rho = -en$ the charge density, we can write the Poisson potential as

$$\nabla^2 V = -4\pi\rho_1 = 4\pi e\, n_1 = 4\pi e\, n_0 \left[\exp(eV/k_B T) - 1\right]$$

letting $n_1 = n - n_0$.

Defining

$$\Phi = \frac{eV}{k_B T}$$

we can write the Poisson potential in this way

$$\nabla^2 \Phi = 4\pi e\, n_0 \frac{e}{k_B T} \left[\exp(\Phi) - 1\right] \tag{1.1}$$

Introducing the classical electron radius

$$r_c = \frac{e^2}{m_e c^2}$$

equation 1.1 becomes

$$\nabla^2 \Phi = \frac{4\pi r_c n_0 m_e c^2}{k_B T} = \lambda_D^{-2} \left[\exp(\Phi) - 1\right] \tag{1.2}$$

where we defined the *Debye length* as

$$\lambda_D^2 = \frac{1}{4\pi r_c n_0} \frac{k_B T}{m_e c^2} \tag{1.3}$$

In a one spatial dimensional world, eq. 1.2 can be integrated. In our 3-dimensional world, we can only obtain a solution spherically symmetric. Remembering that the radial part of the Laplacian, in polar coordinates, is written as

$$\nabla^2 = r^{-1} \frac{\partial^2}{\partial r^2} r$$

and assuming $r' = r/\lambda_D$, eq. 1.2 becomes

$$\frac{d^2}{dr'^2}(r\Phi) = r' \left[\exp(\Phi) - 1\right] \tag{1.4}$$

For small charge imbalances, $\Phi \ll 1$, we have

$$\frac{d^2}{dr'^2}\left(r'\Phi\right) - r'\Phi = 0$$

and its solution is given by

$$\Phi = C\frac{e^{-r'}}{r'} \qquad\qquad V = Q\frac{e^{-r/\lambda_D}}{r}$$

in which Q is a constant. Let's call $q(r)$ the charge within a sphere of radius r and let's apply the Gauss theorem to calculate it. We denote with $S(r)$ a sphere of radius r centred in the origin of the axes and with Σ its surface. Then the charge contained within the sphere can be expressed by

$$q(r) = \int_{S(r)} \rho(r')d\mathbf{r} = \frac{1}{4\pi}\int_{S(r)} \mathrm{div}\mathbf{E}\; d\mathbf{r} = \frac{1}{4\pi}\int_{\Sigma(r)} \mathbf{E}\cdot\frac{\mathbf{r}}{r}d\sigma = r^2 E_r(r)$$

In the case of a shielded potential, we have

$$E_r(r) = -\frac{\partial V}{\partial r} = Qe^{-r/\lambda_D}\left(\frac{1}{\lambda_D r} + \frac{1}{r^2}\right)$$

We obtain $q(0) = Q$ and so the charge density can be written as a regular part ρ_{reg} plus a singularity that corresponds to the point charge in the origin $\rho_{\mathrm{sing}} = Q\delta(\mathbf{r})$.

$$\rho(\mathbf{r}) = Q\delta(\mathbf{r}) + \rho_{\mathrm{reg}}$$

We now write

$$q(r) = Q + q_{\mathrm{reg}}(r) \qquad\qquad q_{\mathrm{reg}}(r) = \int_{S(r)} \rho_{\mathrm{reg}}(r')d\mathbf{r}$$

and, analogously,

$$E_r(r) = \frac{Q}{r^2} + E_{\mathrm{reg}}(r)$$

where it's evident that the regular contribute of the charge density goes to zero when $\lambda_D \to \infty$.

So we get

$$q(0) = Q \qquad\qquad q(\infty) = 0$$

according to the fact that if we put a charge $+Q$ in 0 we must also distribute an opposite charge $-Q$ in the whole surrounding space.

We now note that density $\rho(\mathbf{r})$ is now defined by

$$\rho(\mathbf{r}) = Q\delta(\mathbf{r}) + \rho_{\text{reg}} \qquad \rho_{\text{reg}} = \frac{q'(r)}{4\pi r^2} = -\frac{Qe^{-r/\lambda_D}}{4\pi\lambda_D r^2}$$

The contribution from the regular part is zero when $\lambda_D \to \infty$. In this limit, only the singularity given by the charge Q in the origin survives.

1.4.4 Plasma waves

When studying laser acceleration, we consider an adimensional parameter given by the ratio between the rest electron energy and the electromagnetic field energy:

$$a = \frac{eA}{m_e c^2} \tag{1.5}$$

We can also define a similar a_p in which the mass of the electron is replaced with the mass of the proton.

An electromagnetic wave that propagates into a plasma excites density waves. We can see that from these equations:

$$\begin{cases} \dfrac{\partial n}{\partial t} + \dfrac{\partial}{\partial x_i}(v_i n) = 0 \\ \rho \dfrac{dv_i}{dt} = neE_i \\ \dfrac{\partial E_i}{\partial x_i} = 4\pi ne \end{cases} \tag{1.6}$$

the first one is the continuity equation, the second one follows the conservation of linear momentum and the third one is the Poisson's equation; $\frac{d}{dt}$ is the Eulerian derivative, so that

$$\frac{d}{dt} = \frac{\partial}{\partial t} + \sum_k v_v \frac{\partial}{\partial x_k}$$

Equilibrium requires that $n = n_0$ and $\mathbf{v} = 0, E = 0$. A disturbance in the density, measured as n_1, creates a field $\mathbf{E_1}$ and a drift $\mathbf{v_1}$ of the charged particles, so that now

$$n = n_0 + n_1 \qquad \mathbf{E} \equiv \mathbf{E_1} \qquad \mathbf{v} \equiv \mathbf{v_1}$$

Keeping in mind that $\rho = m_e n$ the equations 1.6 become

$$\begin{cases} \dfrac{\partial n_1}{\partial t} + n_0 \dfrac{\partial v_i}{\partial x_i} = 0 \\ m_e \dfrac{dv_i}{dt} = eE_i \\ \dfrac{\partial E_i}{\partial x_i} = 4\pi n_1 e \end{cases} \tag{1.7}$$

Deriving the first equation by t and the second by x_i, we get

$$\frac{\partial^2 n_1}{\partial t^2} = -n_0 \frac{\partial^2 v_i}{\partial t \partial x_i} = -\frac{n_0 e}{m_e} \frac{\partial E_i}{\partial x_i} \tag{1.8}$$

The third equation of 1.6 becomes

$$\frac{\partial^2 n_1}{\partial t^2} + \omega_p^2 n_1 = 0$$

in which

$$\omega_p^2 = \frac{4\pi e^2 n_0}{m_e} \tag{1.9}$$

is the plasma frequency. Using the classical electron radius

$$r_e = \frac{e^2}{m_e c^2} = 3 \cdot 10^{-13} \text{ cm}$$

then 1.9 can be written as

$$\omega_p^2 = 4\pi r_e c^2 n_0 \tag{1.10}$$

1.4.5 Refraction index

In linear approximation (electron density perturbations are small and so plasma oscillations are harmonics of x^2 potential type) we can note that the medium becomes optically active and its refraction index can be calculated. Let's consider fields in linear approximation, too. So these equations are valid:

$$\begin{cases} \nabla \times \mathbf{B} = \dfrac{4\pi}{c}\mathbf{j} + \dfrac{1}{c}\dfrac{\partial \mathbf{E}}{\partial t} \\ m\dfrac{\partial \mathbf{v}}{\partial t} = e\mathbf{E} \\ \mathbf{j} = n_0 e \mathbf{v} \end{cases} \tag{1.11}$$

We can choose periodic solutions

$$\mathbf{B} = \mathbf{B}_* e^{-i\omega t} \quad \mathbf{E} = \mathbf{E}_* e^{-i\omega t} \quad \mathbf{D} = \mathbf{D}_* e^{-i\omega t} \quad \mathbf{v} = \mathbf{v}_* e^{-i\omega t} \quad \mathbf{j} = \mathbf{j}_* e^{-i\omega t}$$

so that

$$\nabla \times \mathbf{B}_* = \frac{4\pi}{c}\frac{n_0 e}{m}\frac{\mathbf{E}_*}{-i\omega} + \frac{-i\omega}{c}\mathbf{E}_* = -i\omega \mathbf{E}_* \left(1 - \frac{4\pi e^2 n_0}{m\omega^2}\right) \equiv -i\omega \mathbf{D}_*$$

The Maxwell equation becomes

$$\nabla \times \mathbf{B} = \frac{1}{c}\frac{\partial \mathbf{D}}{\partial t} \qquad \mathbf{D} = \epsilon \mathbf{E} = n_{\text{refr}}^2 \mathbf{E}$$

in which

$$n_{\text{refr}} = \left(1 - \frac{\omega_p^2}{\omega^2}\right)^{\frac{1}{2}}$$

Dispersion relationships

The refraction index is given by the ratio between the group velocity and the vacuum light speed

$$n_{\text{refr}} = \frac{v_G}{c} \tag{1.12}$$

from which we get, having said $\omega = \omega(k)$ the dispersion relationship,

$$v_G = \frac{d\omega}{dk} = cn_{\text{refr}} = c\left(1 - \frac{\omega_p^2}{\omega^2}\right)^{\frac{1}{2}}$$

From here we obtain

$$kc = \int_{\omega_p}^{\omega} \frac{\omega' d\omega'}{\left(\omega'^2 - \omega_p^2\right)^{\frac{1}{2}}} = \frac{1}{2}\int_{\omega_p^2}^{\omega^2} \frac{d\omega'^2}{\left(\omega'^2 - \omega_p^2\right)^{\frac{1}{2}}} = \left(\omega^2 - \omega_p^2\right)^{\frac{1}{2}} \tag{1.13}$$

and

$$k^2c^2 = \omega^2 - \omega_p^2 \tag{1.14}$$

1.4.6 Critical density and skin depth

We note that if $\omega < \omega_p$, the refraction index and the wave number turn into imaginary. There is no wave propagation any more, only a vanishing wave exponentially damped. For a fixed frequency of the electromagnetic wave, the density for which we have $\omega_p = \omega$ is called critical density n_c. For $n > n_c$ the plasma becomes opaque: the e.m. fields are dumped on a characteristic length ℓ_s.

The critical density is defined, using 1.10, by

$$\omega_{cr}^2 \equiv 4\pi r_e c^2 n_{cr} \tag{1.15}$$

so that

$$n_{cr} = \frac{\omega_{cr}^2}{4\pi c^2 r_e} \tag{1.16}$$

Using the known relation

$$\lambda = \frac{2\pi}{k} = \frac{2\pi v}{\omega} \qquad \longrightarrow \qquad \lambda_{cr}^2 = \frac{4\pi^2 c^2}{\omega_{cr}^2} \tag{1.17}$$

we get

$$n_{cr} = \frac{\pi}{\lambda_{cr}^2 r_e} = \frac{3.14}{3 \times 10^{-13} 10^{-8} \lambda^2[\mu\text{m}]} = \frac{10^{21}}{\lambda^2[\mu\text{m}]}\text{cm}^{-3} \tag{1.18}$$

If our density is above the critical one, $n > n_{cr}$, we can define a *skin depth* as follows:

$$\mathbf{E} = \mathbf{E_0} e^{i(kx-\omega t)} = e^{-i\omega t} e^{-x/\ell_s} \tag{1.19}$$

in which $\ell_s = i/k$.

Following from 1.14 we can write

$$k = \frac{1}{c}\left(\omega^2 - \omega_{cr}^2\right)^{1/2} = \frac{i}{\ell_s} \tag{1.20}$$

so that

$$\ell_s = \frac{ic}{(\omega^2 - \omega_{cr})^{1/2}} = \frac{c}{(\omega_{cr} - \omega^2)^{1/2}} \tag{1.21}$$

Using these results, we can write 1.21 as

$$\ell_s = \frac{c}{\left(\omega_p^2 - \omega^2\right)^{1/2}} = \frac{c}{\omega}\left(\frac{\omega_p^2}{\omega^2} - 1\right)^{-1/2} = \frac{\lambda}{2\pi}\left(\frac{\omega_p^2}{\omega^2} - 1\right)^{-1/2} \tag{1.22}$$

Calculating the ratio between ω_p and ω using 1.10 and 1.15 we get that $\omega_p^2/\omega^2 = n_e/n_{cr}$

$$\ell_s = \frac{\lambda}{2\pi}\left(\frac{n_e}{n_{cr}} - 1\right)^{-1/2}$$

If $\omega_p \gg \omega$, so that $n_e \gg n_{cr}$, we have

$$\ell_s \approx \frac{\lambda}{2\pi}\frac{n_{cr}}{n_e} = \frac{\lambda\omega}{2\pi\omega_p} = \frac{c}{\omega_p} \tag{1.23}$$

1.5 Protons acceleration

Acceleration of particles through laser pulses got a substantial progress in the last years, thanks to the dramatic increase of power obtained with the CPA (chirped pulse amplification). The protons and ions acceleration, after the first studies with the high energy Nd:glass lasers, has been developed using the low energy (but high power) Ti:Sa lasers [8].

The protons beam quality was initially very poor, but subsequent improvements (microstructured targets, energy crossing the 10 MeV line) made possible to propose the use of laser accelerated protons for therapy, even though many studies are still required before the laser accelerated proton beams can be delivered to patients [9].

Recently, also CO_2 lasers have been used: they have a very long wavelength, native circular polarization and a relatively good conversion efficiency. The problem with them is

their long pulse duration mixed with a low power, but both aspects are now finding new people willing to improve them thanks to recent interesting results [10].

There are two main laser regimes that produce protons acceleration: TNSA (Target Normal Sheath Acceleration) and RPA (Radiation Pressure Acceleration).

1.5.1 Target Normal Sheath Acceleration

Most of the experiments about laser-plasma ion acceleration exploited this regime, focusing an intense laser pulse on a target with overcritical electron density (i.e. plasma formed by the ionization of a solid) with a high thickness ($\ell > \ell_s$). Many experiments, also, consider non-normal incidence on the target foil.

The acceleration happens because electrons in the first layers get excited and become hot for a thickness of a few ℓ_s. These electrons have an essentially diffusive motion, both in the laser direction and in the opposite one.

The electrostatic field created by the charge imbalance accelerates the ions [11]. Being the diffusion quite isotropic, the accelerating fields experienced by the ions are strongest on the surfaces of the foil and normal to them, on both sides of the target. We also get a lot of angular dispersion, with two main peaks on both rear and front direction along the laser beam. The electrons cloud has a thickness of a few Debye lengths.

Let's consider a pulse propagating along z axis, polarized along y. Conjugated momenta are:

$$P_x = p_x \qquad P_y = p_y - \frac{eA_y}{c} = p_y - m_e c a \qquad P_z = p_z$$

Kinetic energy of an electron is given by:

$$T = m_e c^2(\gamma - 1) = m_e c^2 \left[\left(1 + \frac{\mathbf{p}^2}{m_e^2 c^2} \right)^{1/2} - 1 \right] \tag{1.24}$$

If $\mathbf{A} = A_y(z)\mathbf{e}_y$ were the vector potential of a fixed external field, then P_y would be conserved exactly and would be zero because before the waves arrives we have $A_y = p_y = 0$. Because of the fluid nature of this problem, we can only say that $P_y = 0$; coupled with $p_y = m_e c a$ and $p_z = p$, we can write the 1.24 as

$$T = m_e c^2 \left[\left(1 + \frac{p^2}{m_e^2 c^2} + a^2 \right)^{1/2} - 1 \right] \tag{1.25}$$

If no fields, other than those generated by $\mathbf{A}$, are there, then the longitudinal acceleration is given by the ponderomotive force. Let's see how a longitudinal force comes out: starting

from a quickly oscillating $A_y(z)$, we can write

$$\langle A(z,t)\rangle = 0 \qquad\qquad \left\langle A^2(z,t)\right\rangle \neq 0$$

Writing the Lagrangian

$$L = \frac{m_e}{2}\mathbf{v}^2 + \frac{e}{c}v_y\ A_y(z)$$

we obtain

$$P_x = m_e\dot{x} \qquad\qquad P_y = m_e\dot{y} + \frac{e}{c}A_y$$

The Hamiltonian is

$$\begin{aligned} H &= \frac{1}{2m_e}\left[P_x^2 + \left(P_y - \frac{e}{c}A_y\right)^2 + P_z^2\right] = \\ &= \frac{1}{2m_e}\left[P_x^2 + P_y^2 + P_z^2 - 2\frac{e}{c}A_yP_y + \frac{e^2}{c^2}A_y^2\right] \end{aligned} \tag{1.26}$$

$$\dot{x} = \frac{P_x}{m_e} \quad \dot{y} = \frac{P_y}{m_e} - \frac{e}{m_ec}A_y \quad \dot{z} = \frac{P_z}{m_e}$$

$$\ddot{z} = \dot{P}_z = -\frac{e^2}{c^2}\frac{\partial}{\partial_z}\left\langle A_y^2\right\rangle \tag{1.27}$$

The longitudinal motion is collective, while the transverse motion can be considered as thermal agitation (it will be suppressed in RPA regime as we will see).

Poisson-Boltzmann equation

The main role in the ion acceleration, so, is played by the *hot* electron component. The relativistically strong laser pulse transfers its energy and momentum to electrons, that are accelerated up to an energy of the order of magnitude of the laser ponderomotive potential.

The efficiency, η_e, of the energy conversion from laser to hot electrons should be of the order of 20%-30%, but no real according exists in literature. After crossing the target, the electrons distribute themselves over few Debye lengths $\lambda_{e,\mathrm{hot}}$, which for $n_{e,\mathrm{hot}} = 3\ 10^{19}$ cm^{-3} and $E_{e,\mathrm{hot}} = 6$ MeV is $\lambda_{e,\mathrm{hot}} = 3\ \mu$m. But let's consider this model in detail.

If we have a one dimensional slab along z, extending from $z = 0$ (the position of the solid-vacuum interface at the rear side of the target before the arrival of the pulse) up to $x = h$ (the farther limit of the electron cloud, that will be determined later), we could assume that the *hot* electron density follows the Boltzmann distribution

$$n_e(z) = n_0 \exp\left[\frac{eV}{k_BT}\right] \tag{1.28}$$

where $V = V(z)$ is the electrostatic potential, n_0 is the value of the hot electron density at $V = 0$ and T is the constant temperature of the electrons produced by the laser pulse.

This is, of course, a simplification, as it would be better to use a more complicated electron distribution function [12].

By assuming that, over the electron time scale, the ion distribution remains localized (immobile ions), the Poisson-Boltzmann equation in the "vacuum" region, that is for $z \geq 0$, reads

$$\frac{d^2V}{dz^2} = 4\pi\ e\ n_0\ \exp(eV/k_BT) \tag{1.29}$$

A problem arise, because the rhs of 1.28 does not vanish for $z \to +\infty$, unless $V(+\infty) \to -\infty$. This situation is not acceptable, because any positively charged particle at $z = 0$ would be accelerated indefinitely in such a potential distribution. We must introduce an upper boundary h, chosen on the basis of the electron energy conservation [13]: the kinetic energy acquired by a test electron from the laser pulse should be equal to the work done from the electron to cover the distance h in the presence of the spatial distribution of the other fast electrons. It results:

$$h = \sqrt{\frac{\gamma_e - 1}{\pi r_c n_{av}}}$$

in which r_c is the usual classical electron radius, γ_e is the relativistic factor of the test electron and n_{av} is the average density of hot electrons.

Equation 1.29, coupled with eq. 1.28, is then solved with boundary conditions $V(h) = 0$ and $V'(h) = 0$. These conditions mean that $n_e(h) = n_0$ and $n_e(z > h) = 0$, so that there's a discontinuity in the electron distribution at $z = h$. However, due to the other boundary condition, the corresponding electric field profile is continuous, being zero at $z = h$.

Defining

$$\Phi = \frac{eV}{k_BT} \qquad \zeta = \frac{z}{\lambda_D} \qquad \eta = h/\lambda_D \tag{1.30}$$

and using $k_B = 1$ going on, the equation 1.29 becomes

$$\frac{d^2\Phi}{d\zeta^2} = e^{\Phi} \tag{1.31}$$

To solve it, we must use, as we previously said, $\Phi(\eta) = \Phi'(\eta) = 0$. The prime integral of the motion, noting that the potential is $-e^{\Phi}$ and so not forgetting conditions at $\zeta = \eta$, is

$$\frac{1}{2}\left(\frac{d\Phi}{d\zeta}\right)^2 - e^{\Phi} = -1$$

so that

$$\sqrt{2}\int_{\eta}^{\zeta} d\zeta' = \int_0^{\Phi} \frac{d\phi}{\sqrt{e^{\phi} - 1}} \tag{1.32}$$

Using $u = e^{\phi}$ we get

$$\sqrt{2}(\zeta - \eta) = 2 \int_1^{e^{\phi}} \frac{d\sqrt{u-1}}{u}$$

Inserting now $w = \sqrt{u-1}$

$$\frac{\zeta - \eta}{\sqrt{2}} = \int_0^{\sqrt{e^{\phi}-1}} \frac{dw}{1+w^2} = \arctan \sqrt{e^{\phi}-1}$$

$$\Phi = \log\left(1 + \tan^2\left(\frac{\zeta - \eta}{\sqrt{2}}\right)\right)$$

Going back to original quantities, using the 1.30 relations, we have

$$V(z) = \frac{T}{e} \log\left(1 + \tan^2\left(\frac{h-z}{\lambda_D\sqrt{2}}\right)\right)$$

The electric field is

$$\varepsilon_z = -V'(z) = \frac{T}{e}\frac{\sqrt{2}}{\lambda_D} \tan\frac{h-z}{\lambda_D\sqrt{2}}$$

It's now easy to get the maximum energy:

$$E_{\max} = Ze\,V(0) = ZT \log\left(1 + \tan^2\left(\frac{h}{\lambda_D\sqrt{2}}\right)\right) \tag{1.33}$$

Experimental results are different from these calculations: electrons energy depends not only on laser intensity but also on its energy and duration. Passoni [14] developed a more realistic model, with cold and hot electron populations, slow heavy ions and fast lighter ones, to describe metals with a small hydrogen rich surface.

1.5.2 Radiation Pressure Acceleration

Radiation Pressure Acceleration (RPA) is a viable method to obtain ions up to energies of some GeV/nucleon, and so up to the relativistic domain. It's an alternative route to the better understood TNSA regime; it has been developed and stimulated by simulations of Esirkepov et al. [15, 16], in which they show that at intensities $I > 5 \times 10^{21}$ W/cm^2 RPA starts to dominate over TNSA.

It's a different mechanism, particularly enlightened with circularly polarized laser pulses: in such conditions, the acceleration of "fast" electrons at the laser–plasma interface is almost suppressed, ruling out TNSA which is driven from the space charge produced by energetic

electrons escaping in vacuum. Electrons heating become negligible: it's the ponderomotive force that acts directly accelerating electrons and ions in the RPA regime [17].

A simple minimal model to show the role of the polarization in laser interaction with an overdense plasma can be described as follows: let's assume a plane, elliptically (circularly if $\epsilon = 1$) polarized wave of frequency ω. It's incident on an overdense plasma with a step–like profile of the electron density ($n_e(x) = n_0\,\theta(x)$). We assume $\omega_p > \omega$, being $\omega_p = \sqrt{4\pi n_0 e^2/m_e}$ the plasma frequency.

For sufficiently low intensity the vector potential inside the plasma can be written as

$$\mathbf{A}(z,t) = \frac{A(0)}{\sqrt{1+\epsilon^2}} e^{-z/\ell_s} \left(\hat{x}\cos\omega t + \epsilon\hat{y}\sin\omega t\right) \tag{1.34}$$

where $\ell_s = c/\sqrt{\omega_p^2 - \omega^2}$ (1.22) and ϵ is the ellipticity ($0 < \epsilon < 1$).

The longitudinal force on electrons due to the $\mathbf{v}\times\mathbf{B}$ term is then obtained, like in 1.27, as

$$F_z = -\frac{e^2}{2m_e c^2}\partial_z \mathbf{A}^2 = F_0 e^{-2z/\ell_s}\left(1 + \frac{1-\epsilon^2}{1+\epsilon^2}\cos 2\omega t\right)$$

So, from a microscopic point of view, P_{rad} (radiation pressure) is given by the integral of temporal average of the Lorentz's law $\mathbf{F} = \mathbf{J}\times\mathbf{B}$ over a period of the electromagnetic field and over the target volume. Since this ponderomotive force (its density is called $\mathbf{f}_p$) scales with the inverse of the particle mass, its effects on ions are negligible. In fact, the transfer of momentum to ions is actually mediated by the electrostatic field generated by the displacement of the electrons under the action of $\mathbf{f}_p$ [18].

If $\mathbf{f}_p$ and the electrostatic force on electrons coming from unmoved ions balance each other, so that we can say that the electrons are in a mechanical equilibrium, the total electrostatic pressure P_{es} on ions is given by the integral of $Zen_i\mathbf{E}_{\text{es}}$. If the condition of quasi-neutrality $Zen_i = en_e$ holds, then $Zen_i\mathbf{E}_{\text{es}} = en_e\mathbf{E}_{\text{es}} = \mathbf{f}_p$, yielding $P_{\text{es}} = P_{\text{rad}}$. In these conditions one can effectively assume that the target ions are pushed by P_{rad}

We have two models for this regime, depending on the thickness of the target: the Hole Boring (HB) model, for thicker targets, and the Light Sail (LS) model, for thinner ones.

Hole Boring Regime

The model is best described with the help of the figure 1.2. The first frame (a) corresponds to the initial stage in which the electrons have piled up under the action of the radiation pressure, creating the space-charge field E_x, which balances the ponderomotive force. We can say that electrons are in equilibrium and ions did not move significantly. So we can describe E_x and n_e with those simple profiles, that approximate the exact profiles calculated in steady conditions [19].

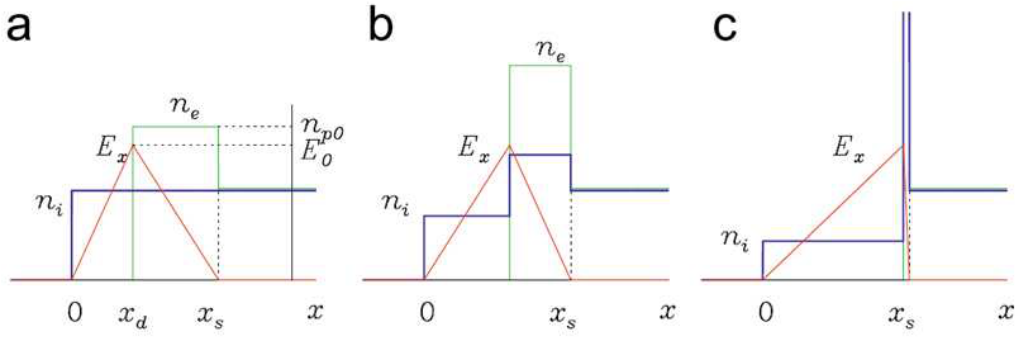

Figure 1.2: *Profiles of the ion density n_i (blue), electron density n_e (green) and electrostatic field E_x (red) at three different stages of ion acceleration [17].*

Given the original expression by J. C. Maxwell

$$P_{\text{rad}} = (1+R)\frac{I}{c} \tag{1.35}$$

the model parameters x_d, E_0 and n_{p0} shown in 1.2 are related to each other by the Poisson equation, the law of charge conservation and the equilibrium condition.

$$P_{\text{es}} = \int en_e E_x dx \doteq P_{\text{rad}} = 2\frac{I}{c}$$

when we assume total reflection ($R = 1$). The penetration distance of the ponderomotive force into the target is $\ell_s = x_s - x_d$ and is of the order of the collisionless skin depth $d_p = c/\omega_p$ (ω_p is the plasma frequency). This simple profile allows us to solve motion equations analytically: we easily find that all ions in this region get to x_s at the same time, with an energy spectrum that is a flat-top distribution extending from zero to the cut-off value of

$$E_{\text{max}} = \frac{m_p}{2}v_m^2 = 2m_p c^2 \Pi \tag{1.36}$$

where

$$\frac{v_m}{c} = 2\Pi^{1/2}, \qquad \Pi = \frac{v_m^2}{4c^2}, \qquad \Pi = \frac{I}{m_i n_i c^3} = \left(\frac{Z}{A}\right)\frac{n_c}{n_e}\frac{m_e}{m_p}a_0^2.$$

(a_0 is the dimensionless pulse amplitude corresponding to the field intensity I (for circular polarization), A is the atomic mass number).

What we observe from simulations is that the fastest ions form a narrow bunch of velocity v_m that penetrated into the overdense plasma. The other ions form another peak moving with a velocity $v_b = v_m/2$. Simply, we can say that v_b is the speed at which a hole is bored into the plasma.

In [20, 21, 22] they propose a relativistic variant of 1.36. The main point is the use of momentum conservation in the reference frame that is co-moving with the target surface. In this reference frame, the intensity is $I' = I\,(1 - v_b/c)\,/\,(1 + v_b/c)$ or, using $\beta = v_b/c$, $I' = I(1-\beta)/(1+\beta)$.

Using this relation, they found this new form of the equation:

$$E_{\max} = 2m_p c^2 \frac{\Pi}{1 + 2\Pi^{1/2}} \tag{1.37}$$

This means that the transfer of energy from EM wave to the plasma, in the laboratory frame of reference, occurs because of the frequency redshift of each photon that is reflected from the moving surface of the plasma. This energy is proportional to the relative shift, and like the intensity we get $\omega'/\omega = (1 - v_b/c)\,/\,(1 + v_b/c)$.

The scaling of the ion energy with the laser intensity and the target density, which can be derived from equations 1.36-1.37, is unfavourable if we aim at relativistic energies. For targets at solid densities, $n_e > 100 n_c$, values of $\Pi \approx 1$ cannot be approached even at the highest intensities available for the next years. To obtain $\Pi \approx 10^{-1}$, that means ≈ 100 MeV per nucleon (useful in hadron-therapy), we must use targets with density of only a few n_c.

To produce ions with energy exceeding 10^2 MeV we must wait for technologies like the few-cycle pulses at ultrahigh intensity.

Light Sail regime

The model of this regime is based on the concept of a totally reflecting plane mirror boosted by a light wave. For long enough values of pulse duration τ_L, such that $v_b \tau_L > \ell$, being ℓ the thickness of the target, the hole boring through the target is "complete" and all the ions are displaced by the radiation pressure. For a very thin target having $\ell \leq \ell_s$ (ℓ_s is the penetration distance of the ponderomotive force into the target) all the ions are accelerated as a single bunch. The average motion of the target can be described as that of a reflecting object boosted by the radiation pressure.

Let's consider a mirror that is moving along the positive direction of the x axis with speed u with respect to the lab frame of reference S. We denote with x^μ the contravariant coordinates in S and x'^μ those in S' co-moving with the mirror.

So we can write:

$$x^0 = ct, \qquad x^1 = x, \qquad x^2 = y, \qquad x^3 = z. \qquad \frac{\partial x'^\alpha}{\partial x^\beta} = L^\alpha_\beta$$

Our convention is to use a Minkowsky metric like the following:

$$g_{\alpha\beta} = \begin{pmatrix} 1 & 0 & 0 & 0 \\ 0 & -1 & 0 & 0 \\ 0 & 0 & -1 & 0 \\ 0 & 0 & 0 & -1 \end{pmatrix}$$

We denote with $\mathbf{x}$ the vector column made by the x^μ and with x_μ the covariant components. The relation between them is this:

$$x_\mu = g_{\mu\nu}x^\nu \qquad x^\mu = g^{\mu\nu}x_\nu \qquad g^{\mu\alpha}g_{\alpha\nu} = \delta^\mu_\nu$$

For the Minkowsky metric tensor we have $g^{\mu\nu} = g_{\mu\nu}$. The relativistic invariance $x'^\mu x'_\mu = x^\mu x_\mu$ can be written as

$$x'^\mu g_{\mu\nu} x'^\nu = x^\mu g_{\mu\nu} x^\nu \qquad \longrightarrow \qquad \mathbf{x}' = L\mathbf{x}$$

$$\mathbf{x}' \cdot g\mathbf{x}' \equiv L\mathbf{x} \cdot gL\mathbf{x} = \mathbf{x} \cdot \tilde{L}gL\mathbf{x}$$

($\tilde{L}$ is the transpose) so that the invariance implies $\tilde{L}gL = g$.

Remembering that

$$\beta = \frac{u}{c} \qquad \gamma = \left(1 - \beta^2\right)^{-1/2}$$

we can write the matrix for the Lorentz transformation along the x axis as

$$L = \begin{pmatrix} \gamma & -\beta\gamma & 0 & 0 \\ -\beta\gamma & \gamma & 0 & 0 \\ 0 & 0 & 1 & 0 \\ 0 & 0 & 0 & 1 \end{pmatrix}$$

It's easy to note that

- $\tilde{L}gL = g$
- $\tilde{L} = L$
- $\det L = 1$
- $L^{-1}(\beta) = L(-\beta)$

Let's compose two Lorentz transformations of this type:

$$L(\beta_1) = \begin{pmatrix} \gamma_1 & -\beta_1\gamma_1 & 0 & 0 \\ -\beta_1\gamma_1 & \gamma_1 & 0 & 0 \\ 0 & 0 & 1 & 0 \\ 0 & 0 & 0 & 1 \end{pmatrix}$$

$$L(\beta_2) = \begin{pmatrix} \gamma_2 & -\beta_2\gamma_2 & 0 & 0 \\ -\beta_2\gamma_2 & \gamma_2 & 0 & 0 \\ 0 & 0 & 1 & 0 \\ 0 & 0 & 0 & 1 \end{pmatrix}$$

$$L(\beta_1) \cdot L(\beta_2) = \begin{pmatrix} \gamma_1\gamma_2 + \beta_1\beta_2\gamma_1\gamma_2 & -\beta_2\gamma_2\gamma_1 - \beta_1\gamma_1\gamma_2 & 0 & 0 \\ -\beta_1\gamma_1\gamma_2 - \beta_2\gamma_1\gamma_2 & \beta_1\gamma_1\beta_2\gamma_2 + \gamma_1\gamma_2 & 0 & 0 \\ 0 & 0 & 1 & 0 \\ 0 & 0 & 0 & 1 \end{pmatrix}$$

If we limit ourselves to consider the first matrix block 2×2, we can rewrite the Lorentz composition in this way:

$$L(\beta_1) \cdot L(\beta_2) = \gamma_1\gamma_2 \begin{pmatrix} 1 + \beta_1\beta_2 & -\beta_1 - \beta_2 \\ -\beta_1 - \beta_2 & 1 + \beta_1\beta_2 \end{pmatrix}$$

Using

$$\beta = \frac{\beta_1 + \beta_2}{1 + \beta_1\beta_2} = \frac{u}{c}$$

in which

$$u = \frac{u_1 + u_2}{1 + u_1u_2/c^2}$$

we can rewrite the composition in this really simple way:

$$L(\beta) = L(\beta_1) \cdot L(\beta_2) = \gamma \begin{pmatrix} 1 & -\beta \\ -\beta & 1 \end{pmatrix}$$

in which γ, thanks to the fact that $\det L(\beta) = 1 = \det L(\beta_1) \cdot \det L(\beta_2)$, has the usual definition

$$\gamma = \frac{1}{\sqrt{1 - \beta^2}} = \frac{1 + \beta_1\beta_2}{\gamma_1\gamma_2}$$

Let's write the usual electromagnetic field tensor

$$F_{\mu\nu} = \partial_\mu A_\nu - \partial_\nu A_\mu = \begin{pmatrix} 0 & -E_x & -E_y & -E_z \\ E_x & 0 & B_z & B_y \\ E_y & -B_z & 0 & B_x \\ E_z & B_y & -B_x & 0 \end{pmatrix}$$

As we know, it's defined so that $F_{\mu\nu} = -F_{\nu\mu}$

If we consider the Lorentz transformation of $F_{\mu\nu}$ we find that

$$F'_{\mu\nu} = L_{\mu\alpha}(-\beta)L_{\nu\beta}(-\beta)F_{\alpha\beta} = L_{\mu\alpha}(-\beta)F_{\alpha\beta}\tilde{L}_{\beta\nu}(-\beta)$$

where we must note that the last term is equal to $L_{\nu\beta}$ thanks to L properties.

$$F' = L(-\beta)FL(-\beta)$$
$$F = L^{-1}(-\beta)F'L^{-1}(-\beta) = L(\beta)F'L(\beta)$$

If we impose that the mirror and the wave move both in the $x > 0$ verse, such that β is positive (remember that the motion is only in the x direction), we find that the electromagnetic field tensor transforms itself in this way:

$$\begin{cases} E'_x = E_x \\ E'_y = \gamma(E_y - \beta B_z) \\ E'_z = \gamma(E_z + \beta B_y) \end{cases} \qquad \begin{cases} B'_x = B_x \\ B'_y = \gamma(B_y + \beta E_z) \\ B'_z = \gamma(B_z - \beta E_y) \end{cases}$$

Analysing a wave linearly polarized that propagates along the x direction we must set

$$\begin{cases} E_x = E_z = 0 \\ B_x = B_y = 0 \\ E_y = E_0 e^{i(kx-\omega t)} \\ B_z = B_0 e^{i(kx-\omega t)} \end{cases}$$

Remember the Maxwell's equation (in the vacuum)

$$\begin{cases} \nabla \cdot \mathbf{E} = \dfrac{\rho}{\epsilon_0} \\ \nabla \times \mathbf{E} = -\dfrac{\partial \mathbf{B}}{\partial t} \\ \nabla \cdot \mathbf{B} = 0 \\ \nabla \times \mathbf{B} = \dfrac{1}{c^2}\dfrac{\partial \mathbf{E}}{\partial t} \end{cases}$$

n.b.: we could also use the following conventions:

$$\begin{cases} \mathrm{rot}\mathbf{E} = -\dfrac{1}{c}\dfrac{\partial \mathbf{B}}{\partial t} & \longrightarrow \dfrac{\partial B_z}{\partial t} = -c\dfrac{\partial E_y}{\partial x} \\ \mathrm{rot}\mathbf{B} = \dfrac{1}{c}\dfrac{\partial \mathbf{E}}{\partial t} & \longrightarrow \dfrac{\partial E_y}{\partial t} = -c\dfrac{\partial B_z}{\partial x} \end{cases}$$

Substituting the plain wave expression, in which $k = \omega/c$, we find that $E_0 = B_0$ and so

$$E_y = B_z$$

The Poynting vector is

$$\mathbf{E} \times \mathbf{B} = \mathbf{e}_x E_y B_z = \mathbf{e}_x E_y^2$$

and it aims to the positive direction of the x axis.

We have found that

$$\begin{cases} E'_x = 0 \\ E'_y = E_y(1-\beta)\gamma \\ E'_z = 0 \end{cases} \qquad \begin{cases} B'_x = 0 \\ B'_y = 0 \\ B'_z = E_y(1-\beta)\gamma \end{cases}$$

Wave intensity is derived from the modulus of the Poynting vector

$$I = E_y B_z = E_y^2 \qquad I' = E'_y B'_z = E'^2_y$$

so that we can write

$$I' = I\gamma^2(1-\beta)^2 = I\frac{1-\beta}{1+\beta}$$

which is consistent with the fact that wave intensity on the mirror decreases if it's moving in the wave direction and verse. I represents the energy flux (in $\mathrm{W/m^2}$) of an electromagnetic field. I divided by the square of the speed of light in free space is the density of the linear momentum of the electromagnetic field. The time-averaged intensity $\langle I \rangle$ divided by the speed of light in free space is the radiation pressure exerted by an electromagnetic wave on the surface of a target; the transferred momentum is exactly its double, $2I/c$. So we can write:

$$\frac{dP}{dt} = F'_x = \frac{2I'}{c} = \frac{2I}{c}\frac{1-\beta}{1+\beta}$$

in which F'_x is the force per unit of surface.

Denoting with μ the mass per unit of surface, we can write

$$\mu \underbrace{\frac{d}{dt}\frac{u}{\sqrt{1-u^2/c^2}}}_{\text{acceleration}} = \frac{2I}{c}\frac{1-\beta}{1+\beta}$$

if we divide by $\mu\, c$ both sides we get:

$$\frac{d}{dt}\frac{\beta}{\sqrt{1-\beta^2}} = \frac{2I}{\mu c^2}\frac{1-\beta}{1+\beta}$$

If we use a wave packet instead of a plain wave we must write

$$\begin{cases} E_y = E_y(x-ct) = \int f(k) e^{ik(x-ct)} dk \\ B_z = E_y \end{cases}$$

and we get the very well known equation for the relativistic mirror (or light sail):

$$\begin{cases} \dfrac{dw}{dt} = \dfrac{\sqrt{1+w^2}-w}{\sqrt{1+w^2}+w}\,\dfrac{2}{\mu c} I(x-ct) \\ \dfrac{dx}{dt} = c\dfrac{w}{\sqrt{1+w^2}} \end{cases}$$

Choosing β as the independent value we get

$$\begin{cases} \dfrac{d\beta}{dt} = \dfrac{2}{\mu c} I(x-ct)\cdot(1-\beta)^2(1-\beta^2)^{1/2} \\ \dfrac{dx}{dt} = c\beta \end{cases}$$

The efficiency is measured in the case of a plane wave as a Doppler effect

$$\frac{w_{\text{out}}}{w_{\text{in}}} = \left(\frac{1-\beta}{1+\beta}\right)^{1/2}$$

Being $\hbar w$ the photon energy coming in and out, we finally get

$$\eta = 1 - \frac{E_{\text{laser-out}}}{E_{\text{laser-in}}} = 1 - \left(\frac{1-\beta}{1+\beta}\right)^{1/2}$$

The mirror problem

The radiation pressure on a thin target in its rest frame, neglecting absorption and at normal incidence, as we saw, is given by

$$P_{\text{thin}} = 2R_{\text{thin}}\frac{I}{c} \tag{1.38}$$

where R_{thin} is the reflectivity of the thin target.

Equation 1.38 is different from the original one for thick target 1.35 because we must consider now the transmitted wave.

The equation for the mirror is given by:

$$\begin{cases} \dfrac{d\beta}{dt} = \dfrac{2I_0}{\mu c} f\left(\dfrac{t-x/c}{\tau_{\text{laser}}} - 1\right)\dfrac{1-\beta}{1+\beta}(1-\beta^2)^{3/2} \\ \dfrac{dx}{dt} = c\beta \end{cases} \tag{1.39}$$

in which μ is the superficial density and f describes the pulse I_0 amplitude, in the interval $0 \le t - x/c \le 2\tau_{\text{laser}}$

We define the laser energy E_{laser} in this way, supposing that S is the surface enlightened by the laser (spatially uniform):

$$E_{\text{laser}} = I_0 S \int_{x/c}^{(x/c)+2\tau_{\text{laser}}} f(t)dt = I_0 S \tau_{\text{laser}} F \tag{1.40}$$

in which F is the fluence (flux integrated over time):

$$F = \int_{-1}^{1} f(u)du \tag{1.41}$$

For example, we can see that choosing a pulse like

$$f(\omega) = \begin{cases} \cos^2 \dfrac{\pi}{2}\omega & |\omega| < 1 \\ 0 & |\omega| \geq 1 \end{cases}$$

we have $F = 1$.

Let's enter adimensional variables:

$$t' = \frac{t}{\tau_{\text{laser}}} \qquad\qquad x' = \frac{x}{c\tau_{\text{laser}}}$$

Using the notation

$$\lambda = \frac{\tau_{\text{laser}}}{\tau} \qquad\qquad \tau = \frac{\mu c^2}{2I_0}$$

the equation 1.39 becomes

$$\begin{cases} \dfrac{d\beta}{dt'} = \lambda f\left(t' - x' - 1\right) \dfrac{1-\beta}{1+\beta}(1-\beta^2)^{3/2} \\ \dfrac{dx'}{dt'} = \beta \end{cases} \tag{1.42}$$

We now choose $w = t' - x' - 1$ and we find that f doesn't change when w is between -1 and 1. So we get:

$$\begin{cases} \dfrac{d\beta}{dt'} = \lambda f(w) \dfrac{1-\beta}{1+\beta}(1-\beta^2)^{3/2} \\ \dfrac{dw}{dt'} = 1 - \beta \end{cases} \tag{1.43}$$

We search the prime integral using the following method:

$$dH = C\left[(1-\beta)d\beta - \lambda f(\omega)\frac{1-\beta}{1+\beta}\left(1-\beta^2\right)^{3/2} d\omega\right] \tag{1.44}$$

If we choose

$$C = (1+\beta)\,(1-\beta)^{-1}\left(1-\beta^2\right)^{-3/2} \tag{1.45}$$

putting 1.45 in 1.44, $\omega \to \omega'$ and $\beta \to \beta'$, we get

$$dH = \lambda f(\omega')d\omega' - \frac{1+\beta'}{(1-\beta'^2)^{3/2}}d\beta' \tag{1.46}$$

Integrating from $\omega = -1$ to ω and from $\beta = 0$ to β we get

$$H = \lambda \int_{-1}^{\omega} f(\omega')d\omega' - \left(\frac{1+\beta}{1-\beta}\right)^{1/2} \tag{1.47}$$

Note that $t = 0$ means $x = 0$ and $\beta = 0$. Those become $\omega = -1$ and $\beta = 0$ for $t' = 0$ in these gauge reduction, so that $H = -1$.

If we proceed through the end of the pulse, where $\omega = 1$ and the speed is at its maximum β_*, we find that

$$\lambda F - \left(\frac{1+\beta_*}{1-\beta_*}\right)^{1/2} = -1 \qquad \longrightarrow \qquad \beta_* = \frac{1+\lambda F^2 - 1}{1+\lambda F^2 + 1} \tag{1.48}$$

Let's define α as

$$\alpha = \lambda F = \frac{2I_0\tau_{\text{laser}}F}{\mu c^2} = \frac{2I_0 S\tau_{\text{laser}}F}{\mu S c^2} = \frac{2E_{\text{laser}}}{E_{\text{mirror@rest}}} \tag{1.49}$$

Putting 1.49 in 1.48 we find

$$\gamma_* - 1 = \frac{\alpha^2}{2+2\alpha} \tag{1.50}$$

Knowing that the kinetic energy of an ion of atomic mass A is

$$T = Am_pc^2(\gamma - 1)$$

we get

$$T_{\text{ion}} = Am_pc^2(\gamma_* - 1) = Am_pc^2\frac{\alpha^2}{2+2\alpha} \tag{1.51}$$

The kinetic energy of the enlightened mirror surface S, whose rest energy is $E_{\text{mirror@rest}} = \mu S c^2$, is

$$T_{\text{mirror}} = E_{\text{mirror@rest}}(\gamma_* - 1) = E_{\text{mirror@rest}}\frac{\alpha}{2}\frac{\alpha}{1+\alpha} = E_{\text{laser}}\frac{\alpha}{1+\alpha} \tag{1.52}$$

The result would have been the same using $T_{\text{mirror}} = T_{\text{ion}} \cdot N_{\text{ions}}$, where $N_{\text{ions}} = \mu S/(Am_p)$. The efficiency of this regime is

$$\eta = \frac{T_{\text{mirror}}}{E_{\text{laser}}} = \frac{\alpha}{1+\alpha} \tag{1.53}$$

As we can see, reducing the thickness enhances the efficiency and the ion's energy increases as α. On the other hand, there's an upper limit to the thickness of the target, over that it becomes transparent. The mirror is opaque as long as

$$a < \zeta = \pi \frac{n_e}{n_c} \frac{\ell}{\lambda}$$

The number of protons ($A = 1$) that are into a cylinder with a base diameter S is

$$N_{\text{ions}} = n_e S \ell = \frac{n_e}{n_c} S \ell \frac{\pi}{r_c \lambda^2} = \zeta \frac{S}{\lambda r_c}$$

To avoid transparency we need that

$$N_{\text{ions}} \geq N^*_{\text{ions}} = \frac{S}{\lambda r_c} a$$

The minimum thickness, so, is

$$\ell_* = \frac{N^*_{\text{ions}}}{n_e S} = \frac{a}{n_e \lambda r_c}$$

CHAPTER 2

Integrators

We will analyse, in this chapter, the most important methods to solve ordinary differential equations (ODEs) that describe the evolution of a system. We will limit ourselves to the 2D case: (x, t).

Euler's method

If we need to solve a differential equation like $\dot{x} = f(x, t)$, we can see how, on the right hand side, we have the definition for each and every point $(x, t) \in D$ of the tangent curve to the solution $x(t)$.

Let's illustrate it better: we need to fix an arbitrary integration step τ, reasonably small. After the choice of an initial point (t_0, x_0) we calculate the approximate solution for $t_1 = t_0 + \tau$ calculating $x(t_1) = x(t_0) + \tau f(x_0, t_0)$.

At this point, we know the value (t_1, x_1): we only have to repeat this cycle as long as it's needed.

Of course, we do not have to forget that points calculated are only approximated and the reliability of the method depends on the chosen step and on the error propagation during the cycle. To evaluate better the error we are making, we can analyse the Taylor series and estimate the error at each time step:

$$x(t + \tau) = x(t) + \tau \dot{x}(t) + O(\tau^2)$$

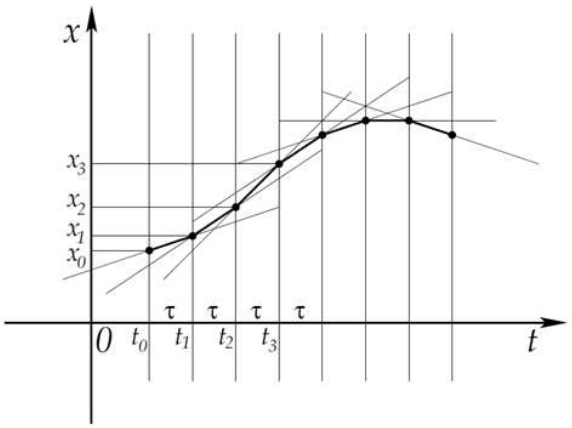

Figure 2.1: *Euler's integration method: we approximate the curve with straight lines, adding a fixed quantity τ to t at each step*

Each and every time step we are neglecting a remainder $O(\tau^2)$.

Note: to use the Taylor expansion, we need that $\dot{x}(t)$ belongs to C^1 class for its arguments, because we're requiring that $x(t)$ can be derived two times.

But how could I use this value to obtain the global error that I'm doing? It seems that we do not have any hint on this.

Let's obtain the effective error done in many steps:

- k-order error [23]:

$$e_k \leq (\Delta t)^m \frac{M}{L} \left[e^{Lt_k} - 1 \right]$$

- Symplectic algorithm: no [23].

Let's design a program[1], using Wolfram Mathematica, that generate a numerical solution to a first order initial value problem of the form

$$y' = f(x, y) \qquad\qquad y(x_0) = y_0$$

using Euler's method.

```
euler[f_, {x_, x0_, xn_}, {y_, y0_}, steps_] :=
 Block [
  {
   xold = x0,
```

[1] http://calculuslab.deltacollege.edu/ODE/7-C-1/7-C-1-b-ma.html

```
  yold = y0,
  sollist = {{x0, y0}},
  x,
  y,
  h
 },
 h = N[(xn - x0)/steps];
 Do
 [
  xnew = xold + h;
  ynew = yold + h*(f /. {x -> xold, y -> yold});
  sollist = Append[sollist, {xnew, ynew}];
  xold = xnew;
  yold = ynew,
  {steps}
 ];
Return[sollist]
]
```

We can try this simple code launching this command, for example:

```
soluzione1=euler[x+2y, {x,0,1},{y,0},40]
```

To enhance the graphical output we can use:

```
MatrixForm[soluzione1]
```

to obtain a table (matrix) form that is simpler to read, or:

```
ListPlot[soluzione1]
```

to obtain a graph with the points, or:

```
ListLinePlot[soluzione1]
```

to get an interpolation of the points and maybe the best possible output.

The parameters are:

- f, for the first order differential equation (in the example the equation is $y' = x + 2y$);
- $x0$, for the initial x value (x_0);

- $y0$, for the initial y value (y_0);
- xn, for the final x value;
- steps, for the number of subdivisions.

The key algorithm consists in finding new x and y values from the previous ones using

$$x_{n+1} = x_n + h \qquad\qquad y_{n+1} = y_n + hf(x_n, y_n)$$

In figure 2.2 there's a visual representation of the results from the example shown above.

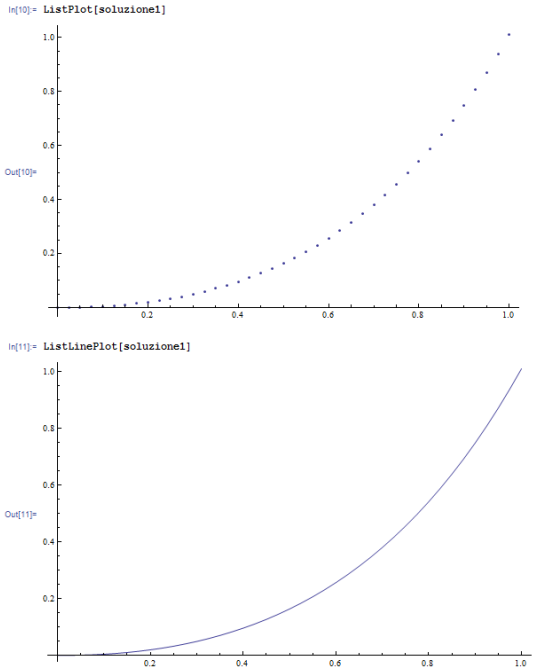

Figure 2.2: *Euler's integration method applied to equation $y' = x + 2y$ using the code described in the chapter 2*

2.1 Runge Kutta schemes

We have just seen an interesting way of solving differential equations of the type $\dot{x} = f(x,t)$ with a second order error:

$$x(t+\tau) = x(t) + \tau\dot{x}(t) + O(\tau^2)$$

We could try to enhance the precision of the algorithm including third order corrections: for example

$$x(t+\tau) = x(t) + \tau\dot{x}(t) + \frac{\tau^2}{2}\ddot{x} + O(\tau^3)$$

But, beyond becoming more strict on requests to our function (it must belong to smoother classes of functions), this method can be really tedious, making everything not feasible. To improve the precision without making more complex numerical and analytical calculations, our calculations can use Runge-Kutta methods. The fundamental idea is to calculate the step between $x(t)$ and $x(t+\tau)$ using the first derivative in a middle point of the interval.

Let's consider a generic function $\phi(t)$. We can see that:

$$\begin{aligned}
\phi(t+\tau) &= \phi\left(t+\frac{\tau}{2}\right) + \frac{\tau}{2}\dot{\phi}\left(t+\frac{\tau}{2}\right) + \frac{\tau^2}{4\cdot 2!}\ddot{\phi}\left(t+\frac{\tau}{2}\right) + O(\tau^3) \\
\phi(t) &= \phi\left(t+\frac{\tau}{2}\right) - \frac{\tau}{2}\dot{\phi}\left(t+\frac{\tau}{2}\right) + \frac{\tau^2}{4\cdot 2!}\ddot{\phi}\left(t+\frac{\tau}{2}\right) + O(\tau^3)
\end{aligned}$$

Subtracting both on the lhs and on the rhs we get

$$\phi(t+\tau) - \phi(t) = \tau\dot{\phi}\left(t+\frac{\tau}{2}\right) + O(\tau^3)$$

The error is a third order one, even if the final calculation only uses first derivative. This happened because subtracting we cancelled the term $\ddot{\phi}$. Summing, on the other hand (or better, on both hand sides!), we get:

$$\phi\left(t+\frac{\tau}{2}\right) = \frac{\phi(t)+\phi(t+\tau)}{2} + O(\tau^2)$$

Also in this case the term $\dot{\phi}$ is lost and we get an order of precision in τ.

There exist many Runge-Kutta methods. Let's look a first one.

Let's replace $x(t)$ to $\phi(t)$ in the subtraction previously done. Remembering that we want to solve the equation $\dot{x} = f(x,t)$, we get the solution

$$x(t+\tau) - x(t) = \tau f\left(x\left(t+\frac{\tau}{2}\right), t+\tau/2\right) \tag{2.1}$$

It's not useful as a solution because it depends on $x(t+\tau/2)$ which is unknown; we still can approximate it with the Euler's method previously seen, so that

$$x(t+\tau/2) = x(t) + \frac{\tau}{2} f\left(x(t), t\right) + O(\tau^2)$$

as can be seen from figure 2.3

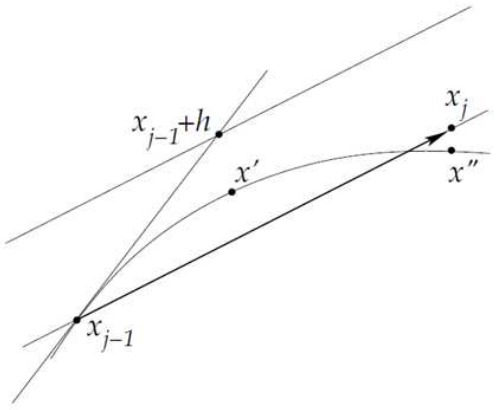

Figure 2.3: *The tangent in the intermediate point x' can be approximated with the tangent at the point $x_{j-1} + h$, calculated with the Euler's method. This markedly reduces the error against the shift along the tangent calculated at x_{j-1}.*

Thanks to this result, we can write the rhs of the 2.1 as:

$$f\left(x\left(t+\frac{\tau}{2}\right), t+\frac{\tau}{2}\right) = f\left(x(t)+\tau f(x(t),t), t+\frac{\tau}{2}\right) + O(\tau^2)$$

Noting that the rhs of the equation 2.1 was multiplied by the factor τ, this approximation still introduces an error of the $\tau O(\tau^2) = O(\tau^3)$ order.

We got a second order Runge-Kutta scheme, with an error of order τ^3.

$$\begin{aligned} h &= \frac{\tau}{2} f\left(x_{j-1}, t_{j-1}\right) \\ x_j &= x_{j-1} + \tau f\left(x_{j-1}+h, t+\frac{\tau}{2}\right) \\ t_j &= t_{j-1} + \tau \end{aligned}$$

To improve the precision, we can use another method: approximate the derivative in the middle point $x\left(t+\frac{\tau}{2}\right)$ calculating the mean between the derivatives at points $x(t)$ and $x(t+\tau)$. The scheme, in this way, becomes:

$$\begin{aligned} h_1 &= \tau f\left(x_{j-1}, t_{j-1}\right) \\ h_2 &= \tau f\left(x_{j-1}+h_1, t_{j-1}+\tau\right) \\ x_j &= x_{j-1} + \frac{h_1+h_2}{2} \\ t_j &= t_{j-1} + \tau \end{aligned}$$

Finally, there exist Runge-Kutta algorithms[2] much much more complex, that reduce the error on the single step; here I wrote the description of a pair of them, the most used.

2.1.1 Third order scheme

(error order: τ^4)

$$\begin{aligned} h_1 &= \tau f\left(x_{j-1}, t_{j-1}\right) \\ h_2 &= \tau f\left(x_{j-1} + \frac{h_1}{2}, t_{j-1} + \frac{\tau}{2}\right) \\ h_3 &= \tau f\left(x_{j-1} + h_2, t_{j-1} + \tau\right) \\ x_j &= x_{j-1} + \frac{h_1}{6} + \frac{2h_2}{3} + \frac{h_3}{6} \\ t_j &= t_{j-1} + \tau \end{aligned}$$

2.1.2 Fourth order scheme

(RK4 - error order: τ^5)

$$\begin{aligned} h_1 &= \tau f\left(x_{j-1}, t_{j-1}\right) \\ h_2 &= \tau f\left(x_{j-1} + \frac{h_1}{2}, t_{j-1} + \frac{\tau}{2}\right) \\ h_3 &= \tau f\left(x_{j-1} + \frac{h_2}{2}, t_{j-1} + \frac{\tau}{2}\right) \\ h_4 &= \tau f\left(x_{j-1} + h_3, t_{j-1} + \tau\right) \\ x_j &= x_{j-1} + \frac{h_1}{6} + \frac{h_2}{3} + \frac{h_3}{3} + \frac{h_4}{6} \\ t_j &= t_{j-1} + \tau \end{aligned}$$

2.2 Symplectic schemes

A Hamiltonian function $H(q,p)$ defines the dynamics of a $2n$-dimensional points system, of coordinates $(q,p) = (q_1, \ldots, q_N, p_1, \ldots, p_N)$. Each point of the set (phase space) represents a possible state of the system.

[2] W. Press, B. P. Flannery, S. A. Teukolsky e W. T. Vetterling. Numerical Recipes in C: The art of scientific computing. Cambridge University Press (1992).

While the system itself evolves from an initial configuration, the states describe in the phase space a curve with a tangent vector defined at each point as $(H_p, -H_q)$; in fact, as we know, the Hamilton's equations

$$\dot{p} = -\frac{\partial H}{\partial q} \qquad\qquad \dot{q} = \frac{\partial H}{\partial p} \tag{2.2}$$

can be interpreted geometrically as the tangent vector of the evolution curve in the phase space (as always, q is the position coordinate and p denotes the momentum).

The time evolution of Hamilton's equations is a symplectomorphism, which means that it preserves the symplectic two-form $dp \times dq$. Simply said, a numerical scheme is a symplectic integrator if it preserves this two-form.

In general, a function f in the phase space is symplectic if and only if

$$f'(z)^T J f'(z) = J$$

in which J is defined as follows:

$$J = \begin{pmatrix} 0 & \mathbb{I}_n \\ -\mathbb{I}_n & 0 \end{pmatrix}$$

Most of the usual numerical methods, like the primitive Euler scheme and the Runge-Kutta scheme, are not symplectic integrators.

How it works: a simple case

Let's assume that the Hamiltonian is separable, so that

$$H(p, q) = T(p) + V(q) \tag{2.3}$$

It's not so rare that a Hamiltonian system can be expressed in this way, fortunately. Let's define $z = (q, p)$ so that

$$\dot{z} = (\dot{q}, \dot{p})$$

Using the formalism $D_H = \{\ , H\}$ eq. 2.2 can be expressed as

$$\begin{aligned} \dot{z} &= J\nabla H(z) = D_H z = \{z, H(z)\} = \frac{\partial(q,p)}{\partial q}\frac{\partial H(q,p)}{\partial p} - \frac{\partial(q,p)}{\partial p}\frac{\partial H(q,p)}{\partial q} = \\ &= (1,0)\frac{\partial H(q,p)}{\partial p} - (0,1)\frac{\partial H(q,p)}{\partial q} = \left(\frac{\partial H(q,p)}{\partial p}, 0\right) - \left(0, \frac{\partial H(q,p)}{\partial q}\right) = \\ &= \left(\frac{\partial H}{\partial p}, -\frac{\partial H}{\partial q}\right) = \left(\frac{\partial T}{\partial p}, -\frac{\partial V}{\partial q}\right) \end{aligned} \tag{2.4}$$

The formal solution of this set of equations is

$$z(\tau) = \exp(\tau D_H) z(0) \tag{2.5}$$

When the Hamiltonian is in the form like 2.3, 2.5 is equivalent to

$$z(\tau) = \exp[\tau(D_T + D_V)] z(0) \tag{2.6}$$

The symplectic integrator scheme approximates this result 2.6 with the product

$$\exp[\tau(D_T + D_V)] = \prod_{i=1}^{k} \exp(c_i \tau D_T) \exp(d_i \tau D_V) + O\left(\tau^{k+1}\right) \tag{2.7}$$

in which c_i and d_i are real numbers and k represents the order of the integrator.

Each of the operators $\exp(c_i \tau D_T)$ and $\exp(d_i \tau D_V)$ is symplectic, so their product appearing in the rhs of the 2.7 is a symplectic map too. From the previous descriptions we can extract many different integrators at different orders, each with its precise set of coefficients c_i and d_i.

But let's see what they give:

$$\exp(c_i \tau D_T) \longrightarrow \begin{pmatrix} q \\ p \end{pmatrix} \mapsto \begin{pmatrix} q' \\ p' \end{pmatrix} = \begin{pmatrix} q + \tau c_i \frac{\partial T}{\partial p}(p) \\ p \end{pmatrix}$$

and

$$\exp(d_i \tau D_V) \longrightarrow \begin{pmatrix} q \\ p \end{pmatrix} \mapsto \begin{pmatrix} q' \\ p' \end{pmatrix} = \begin{pmatrix} q \\ p - \tau d_i \frac{\partial V}{\partial q}(q) \end{pmatrix}$$

An example

If $T = p^2/2m$ and $V = kq^2/2$, we have:

$$\begin{cases} \dfrac{\partial T}{\partial p} = \dfrac{p}{m} = p \text{ if we put } m = 1 \\ \dfrac{\partial V}{\partial q} = kq = F \text{ (this is an example of a spring)} \end{cases}$$

So, knowing that at the first order $c_i = 1$ and $d_i = 1$, we have

$$\begin{cases} q + \Delta t \dfrac{\partial T}{\partial p} = q + \Delta t \cdot p \\ p - \Delta t \dfrac{\partial V}{\partial q} = p + \Delta t \cdot F \end{cases}$$

For other informations, there exist a lot of articles[3]. But let's see an example now.

[3]For example, D. Donnelly, E. Rogers, Symplectic integrators: an introduction, Am. J. Phys. 73 (2005) 10.

Equations of motion

Let's consider a particle that moves in a constant magnetic field $\mathbf{B}$ and in an electric field $\mathbf{E}$ that is orthogonal to $\mathbf{B}$. The equations of motion are:

$$\frac{d\mathbf{r}}{dt} = \frac{\mathbf{p}}{m\gamma} \qquad \frac{d\mathbf{p}}{dt} = e\mathbf{E} + \frac{e}{\gamma c}\mathbf{p} \times \mathbf{B}$$

in which

$$\gamma = \left(1 + \frac{\mathbf{p} \cdot \mathbf{p}}{m^2 c^2}\right)^{1/2}$$

is the relativistic factor.

If we choose that the z axis is along $\mathbf{B}$ and we use the cyclotron frequency

$$\omega_c = \frac{eB}{mc} \tag{2.8}$$

the equations become

$$\frac{d\mathbf{r}}{dt} = \frac{\mathbf{p}}{m\gamma} \qquad \frac{d\mathbf{p}}{dt} = e\mathbf{E} + \frac{\omega_c}{\gamma}\mathbf{p} \times \mathbf{e}_z$$

Let's consider a non-relativistic case. Because $\mathbf{B} = B_z\mathbf{e}_z$ (we choose z along $\mathbf{B}$), we can say that $\mathbf{E} = E_x\mathbf{e}_x + E_y\mathbf{e}_y$. So the equations can be written by components as follows:

$$\dot{x} = \frac{p_x}{m} \qquad \dot{y} = \frac{p_y}{m} \qquad \dot{p}_x = F_x + \omega_c p_y \qquad \dot{p}_y = F_y - \omega_c p_x$$

(we used $\mathbf{F} = e\mathbf{E}$).

The Lagrangian is

$$L = m\frac{\dot{x}^2 + \dot{y}^2}{2} - V(x, y) + \frac{m\omega_c}{2}(x\dot{y} - y\dot{x})$$

The conjugate momenta are

$$P_x = m\dot{x} - \frac{m\omega_c}{2}y \qquad P_y = m\dot{x} + \frac{m\omega_c}{2}x$$

The Hamiltonian is

$$H = \frac{1}{2m}\left[\left(P_x + \frac{m\omega_c y}{2}\right)^2 + \left(P_y + \frac{m\omega_c x}{2}\right)^2\right] + V(x, y)$$

The prime integrals of the motion are H (it doesn't depend on time) and, if the force field $\mathbf{F}$ is central, so that $V = V(r)$, then $L = xP_y - yP_x$ is the second one.

$$H = m\frac{\dot{x}^2 + \dot{y}^2}{2} + V(x, y) \tag{2.9}$$

$$L = xP_y - yP_x = m(x\dot{y} - y\dot{x}) + \frac{m\omega_c}{2}\left(x^2 + y^2\right) \tag{2.10}$$

2.2.1 First order symplectic integrators

Let's consider a simple example, with $m = 1$ and $\mathbf{B} = 0$. So

$$H = T + V \qquad T = \frac{\mathbf{p}^2}{2} \qquad V = V(x)$$

The first order schemes, as we have just seen, can be obtained in this case with splitting variables:

$$\mathbf{x}(t + dt) = e^{\Delta t D_T} e^{\Delta t D_V} \mathbf{x}(t) + O(\Delta t^2) \qquad \mathbf{x} = \begin{pmatrix} \mathbf{r} \\ \mathbf{p} \end{pmatrix} \tag{2.11}$$

or also

$$\mathbf{x}(t + dt) = e^{\Delta t D_V} e^{\Delta t D_T} \mathbf{x}(t) + O(\Delta t^2) \tag{2.12}$$

As before, we can easily obtain the maps for 2.11:

$$\begin{aligned} e^{\Delta t D_V} &\longrightarrow \begin{cases} \mathbf{r}' = \mathbf{r} \\ \mathbf{p}' = \mathbf{p} + \Delta t \mathbf{F}(\mathbf{r}) \end{cases} \\ e^{\Delta t D_T} &\longrightarrow \begin{cases} \mathbf{r}'' = \mathbf{r}' + \mathbf{p}' \Delta t \\ \mathbf{p}'' = \mathbf{p}' \end{cases} \end{aligned} \tag{2.13}$$

Their composition is

$$\begin{cases} \mathbf{p}'' = \mathbf{p} + \mathbf{F}(\mathbf{r}) \Delta t \\ \mathbf{r}'' = \mathbf{r} + (\mathbf{p} + \Delta t \mathbf{F}(\mathbf{r})) \Delta t \end{cases} + O\left(\Delta t^2\right)$$

which can be written as

$$\begin{cases} \mathbf{p}_{n+1} = \mathbf{p}_n + \mathbf{F}(\mathbf{r}_n) \Delta t \\ \mathbf{r}_{n+1} = \mathbf{r}_n + \mathbf{p}_{n+1} \Delta t \end{cases} \tag{2.14}$$

If we are in 1d, writing $\mathbf{F}'(\mathbf{r}_n) = \frac{d\mathbf{F}(\mathbf{r}_n)}{d\mathbf{r}_n}$, it's easy to see that the determinant of the matrix that describes this map is 1:

$$\begin{aligned} \det M &= \det \left(\frac{\partial(\mathbf{r}_{n+1}, \mathbf{p}_{n+1})}{\partial(\mathbf{r}_n, \mathbf{p}_n)} \right) = \\ &= \det \begin{pmatrix} \frac{\partial \mathbf{r}_{n+1}}{\partial \mathbf{r}_n} & \frac{\partial \mathbf{r}_{n+1}}{\partial \mathbf{p}_n} \\ \frac{\partial \mathbf{p}_{n+1}}{\partial \mathbf{r}_n} & \frac{\partial \mathbf{p}_{n+1}}{\partial \mathbf{p}_n} \end{pmatrix} = \\ &= \det \begin{pmatrix} 1 + F' \Delta t^2 & \Delta t \\ F' \Delta t & 1 \end{pmatrix} = \\ &= 1 \end{aligned} \tag{2.15}$$

For 2.12 the map is

$$\begin{cases} \mathbf{r}_{n+1} = \mathbf{r}_n + \mathbf{p}_n \Delta t \\ \mathbf{p}_{n+1} = \mathbf{p}_n + \mathbf{F}(\mathbf{r}_{n+1}) \Delta t \end{cases} \tag{2.16}$$

and the whole treatment is the same.

Action as a generator

An equivalent method would have required discretizing the action:

$$A(q_a, q_b) = \int_{t_a}^{t_b} L(\dot{q}, q, t) dt \tag{2.17}$$

that is the generator that transforms the system from (q_a, p_a) to (q_b, p_b).

So, if we discretize the action and we integrate with a first order method we find the generator of a canonical transformation that defines a first order integrator. Let's consider $t_a = t$, $t_b = t + \Delta t$, $q(t_a) = q_n$ and $q(t_b) = q_{n+1}$. The first derivative of q, $\dot{q} = p$, can be approximated with $(q_{n+1} - q_n)/\Delta t$.

In this way, to solve

$$A(q_n, q_{n+1}) = \int_t^{t+\Delta t} (T(p) - V(q)) dt = \int_t^{t+\Delta t} \left(\frac{\dot{q}^2}{2} - V(q) \right) dt = A_n + O\left(\Delta t^2\right) \tag{2.18}$$

we can use a first order approximation (rectangular):

$$A_n = \frac{(q_{n+1} - q_n)^2}{2\Delta t} - V(q_n) \Delta t \tag{2.19}$$

or

$$A_n = \frac{(q_{n+1} - q_n)^2}{2\Delta t} - V(q_{n+1}) \Delta t \tag{2.20}$$

It's easy to verify from 2.18 that

$$p_n = -\frac{\partial A}{\partial q_n} \qquad \text{and} \qquad p_{n+1} = \frac{\partial A}{\partial q_{n+1}}$$

and so we find this relations for 2.19:

$$p_{n+1} = \frac{\partial A}{\partial q_{n+1}} = \frac{q_{n+1} - q_n}{\Delta t} \qquad \text{and} \qquad p_n = -\frac{\partial A}{\partial q_n} = \frac{q_{n+1} - q_n}{\Delta t} + \frac{dV(q_n)}{dq_n} \Delta t \tag{2.21}$$

$$\begin{cases} \mathbf{p}_{n+1} = \mathbf{p}_n - V'(q_n) \Delta t \\ \mathbf{q}_{n+1} = \mathbf{q}_n + \mathbf{p}_{n+1} \Delta t \end{cases} \tag{2.22}$$

while for 2.20 those are:

$$p_{n+1} = \frac{\partial A}{\partial q_{n+1}} = \frac{q_{n+1} - q_n}{\Delta t} - \frac{dV(q_{n+1})}{dq_{n+1}}\Delta t \qquad \text{and} \qquad p_n = \frac{\partial A}{\partial q_n} = \frac{q_{n+1} - q_n}{\Delta t} \tag{2.23}$$

$$\begin{cases} \mathbf{q}_{n+1} = \mathbf{q}_n + \mathbf{p}_n \Delta t \\ \mathbf{p}_{n+1} = \mathbf{p}_n - V'(q_{n+1})\Delta t \end{cases} \tag{2.24}$$

Extension to B fields

When there's a **B** field the generalization of the previous algorithm is pretty neat at the first order. The two symplectic integrators 2.14 and 2.16 become

$$\begin{cases} \mathbf{p}_{n+1} = \mathbf{p}_n + \mathbf{E}(\mathbf{r}_n)\Delta t + \omega_c \mathbf{p}_n \times \mathbf{e}_z \Delta t \\ \mathbf{r}_{n+1} = \mathbf{r}_n + \mathbf{p}_{n+1}\Delta t \end{cases} \tag{2.25}$$

and

$$\begin{cases} \mathbf{r}_{n+1} = \mathbf{r}_n + \mathbf{p}_n \Delta t \\ \mathbf{p}_{n+1} = \mathbf{p}_n + \mathbf{E}(\mathbf{r}_{n+1})\Delta t + \omega_c \mathbf{p}_{n+1} \times \mathbf{e}_z \Delta t \end{cases} \tag{2.26}$$

in which $\mathbf{E} = \mathbf{E}(\mathbf{r})$ is a central external force.

This second 2.26 integrator, as we can see, is not explicit but it can become so thanks to the fact that it's linear in the momentum. They're not symplectic: to get a symplectic version we have to start from the action, which now is:

$$A_n = \frac{(\mathbf{r}_{n+1} - \mathbf{r}_n)^2}{2\Delta t} - V(\mathbf{r}_n)\Delta t + \frac{\omega_c}{2}\mathbf{r}_n \times (\mathbf{r}_{n+1} - \mathbf{r}_n) \cdot \mathbf{e}_z \tag{2.27}$$

or

$$A_n = \frac{(\mathbf{r}_{n+1} - \mathbf{r}_n)^2}{2\Delta t} - V(\mathbf{r}_{n+1})\Delta t + \frac{\omega_c}{2}\mathbf{r}_{n+1} \times (\mathbf{r}_{n+1} - \mathbf{r}_n) \cdot \mathbf{e}_z \tag{2.28}$$

The equations that we get from these actions are

$$\mathbf{P}_{n+1} = \frac{\partial A}{\partial \mathbf{r}_{n+1}} \qquad \text{and} \qquad \mathbf{P}_n = -\frac{\partial A}{\partial \mathbf{r}_{n+1}} \tag{2.29}$$

in which **P** is not the momentum but

$$\mathbf{P} = \mathbf{p} + \frac{\omega_c}{2}\mathbf{e}_z \times \mathbf{r} \tag{2.30}$$

2.2.2 Second order symplectic integrators

$$\mathbf{x}(t+dt) = \underbrace{e^{\frac{\Delta t}{2}D_V}}_{C}\underbrace{e^{\Delta t D_T}}_{B}\underbrace{e^{\frac{\Delta t}{2}D_V}}_{A}\mathbf{x}(t) + O(\Delta t^3) \qquad \mathbf{x} = \begin{pmatrix} \mathbf{r} \\ \mathbf{p} \end{pmatrix} \tag{2.31}$$

$$\begin{aligned}
A \quad &: \quad \begin{cases} \mathbf{r}' = \mathbf{r} \\ \mathbf{p}' = \mathbf{p} + \frac{\Delta t}{2}\mathbf{F}(\mathbf{r}) \end{cases} \\
A+B \quad &: \quad \begin{cases} \mathbf{r}'' = \mathbf{r}' + \mathbf{p}'\Delta t = \mathbf{r} + \Delta t\left(\mathbf{p} + \frac{\Delta t}{2}\mathbf{F}(\mathbf{r})\right) \\ \mathbf{p}'' = \mathbf{p}' = \mathbf{p} + \frac{\Delta t}{2}\mathbf{F}(\mathbf{r}) \end{cases} \\
A+B+C \quad &: \quad \begin{cases} \mathbf{r}''' = \mathbf{r}'' = \mathbf{r} + \Delta t\left(\mathbf{p} + \frac{\Delta t}{2}\mathbf{F}(\mathbf{r})\right) \\ \mathbf{p}''' = \mathbf{p}'' + \frac{\Delta t}{2}\mathbf{F}(\mathbf{r}'') = \mathbf{p} + \frac{\Delta t}{2}\mathbf{F}(\mathbf{r}) + \frac{\Delta t}{2}\mathbf{F}\left(\mathbf{r} + \Delta t\left(\mathbf{p} + \frac{\Delta t}{2}\mathbf{F}(\mathbf{r})\right)\right) \end{cases}
\end{aligned} \tag{2.32}$$

This can be better written as

$$\begin{cases} \mathbf{r}_{n+1} = \mathbf{r}_n + \mathbf{p}_{n+1}\Delta t + \mathbf{F}(\mathbf{r}_n)\frac{\Delta t}{2} \\ \mathbf{p}_{n+1} = \mathbf{p}_n + \frac{\Delta t}{2}\mathbf{F}(\mathbf{r}_n) + \frac{\Delta t}{2}\mathbf{F}(\mathbf{r}_{n+1}) \end{cases} \tag{2.33}$$

Let's calculate the determinant of the matrix that describes this map:

$$\begin{aligned}
\det M &= \det\left(\frac{\partial(\mathbf{r}_{n+1}, \mathbf{p}_{n+1})}{\partial(\mathbf{r}_n, \mathbf{p}_n)}\right) = \\
&= \det\begin{pmatrix} \frac{\partial \mathbf{r}_{n+1}}{\partial \mathbf{r}_n} & \frac{\partial \mathbf{r}_{n+1}}{\partial \mathbf{p}_n} \\ \frac{\partial \mathbf{p}_{n+1}}{\partial \mathbf{r}_n} & \frac{\partial \mathbf{p}_{n+1}}{\partial \mathbf{p}_n} \end{pmatrix} = \\
&= \det\begin{pmatrix} 1 + \mathbf{F}'(\mathbf{r}_n)\frac{\Delta t^2}{2} & \Delta t \\ \mathbf{F}'(\mathbf{r}_n)\frac{\Delta t}{2} + \frac{\Delta t}{2}\mathbf{F}'(\mathbf{r}_{n+1})\frac{\partial \mathbf{r}_{n+1}}{\partial r_n} & 1 + \frac{\Delta t}{2}\mathbf{F}'(\mathbf{r}_{n+1})\frac{\partial \mathbf{r}_{n+1}}{\partial p_n} \end{pmatrix} = \\
&= \det\begin{pmatrix} 1 + \mathbf{F}'(\mathbf{r}_n)\frac{\Delta t^2}{2} & \Delta t \\ \frac{\Delta t}{2}\left[\mathbf{F}'(\mathbf{r}_n) + \mathbf{F}'(\mathbf{r}_{n+1})\frac{\partial \mathbf{r}_{n+1}}{\partial r_n}\right] & 1 + \frac{\Delta t}{2}\mathbf{F}'(\mathbf{r}_{n+1})\frac{\partial \mathbf{r}_{n+1}}{\partial p_n} \end{pmatrix} = \\
&= \det\begin{pmatrix} 1 + \mathbf{F}'(\mathbf{r}_n)\frac{\Delta t^2}{2} & \Delta t \\ \frac{\Delta t}{2}\left[\mathbf{F}'(\mathbf{r}_n) + \mathbf{F}'(\mathbf{r}_{n+1})\left(1 + \mathbf{F}'(\mathbf{r}_n)\frac{\Delta t^2}{2}\right)\right] & 1 + \frac{\Delta t^2}{2}\mathbf{F}'(\mathbf{r}_{n+1}) \end{pmatrix} = \\
&= 1 + \mathbf{F}'(\mathbf{r}_n)\frac{\Delta t^2}{2} + \frac{\Delta t^2}{2}\mathbf{F}'(\mathbf{r}_{n+1}) + \frac{\Delta t^4}{4}\mathbf{F}'(\mathbf{r}_n)\mathbf{F}'(\mathbf{r}_{n+1}) + \\
&- \frac{\Delta t^2}{2}\left[\mathbf{F}'(\mathbf{r}_n) + \mathbf{F}'(\mathbf{r}_{n+1}) + \frac{\Delta t^2}{2}\mathbf{F}'(\mathbf{r}_n)\mathbf{F}'(\mathbf{r}_{n+1})\right] = \\
&= 1
\end{aligned} \tag{2.34}$$

2.3 Leapfrog integrators

Leapfrog integration is another way to solve ODEs. It is based on calculating positions and velocities at interleaved time points, in such a way that they *leapfrog* over each other.

There exist schemes that are accurate at the second order both in space and time and are computationally light. They are often called staggered leapfrog algorithms.

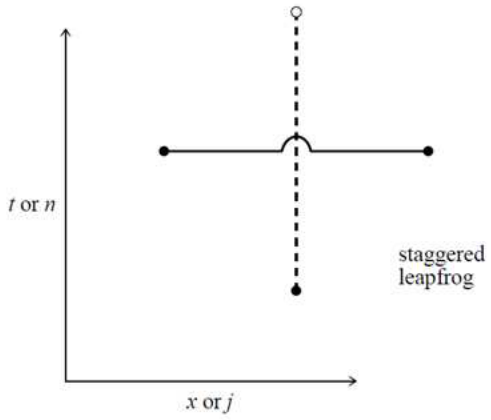

Figure 2.4: *Staggered leapfrog scheme representation. Note that the informations that come from two previous time steps are used to calculate the next step. This scheme is second-order both in x and in t.*

Using values of u_n at time t_n we can calculate currents (fluxes) $F_{j,n}$. Then, we calculate the new values using the flux at the middle point, using the following algorithm:

$$u_{j,n+1} - u_{j,n-1} = -\frac{\Delta t}{\Delta x}\left(F_{j+1,n} - F_{j-1,n}\right)$$

This algorithm requires double the storage: we need to save both u_{n-1} and u_n to calculate u_{n+1}

2.3.1 Second order scheme (LF2)

This algorithm is not exactly symplectic and it also requires the value $\mathbf{p}_{-1/2}$ that needs to be calculated with a Taylor expansion.

$$\begin{cases} \mathbf{p}(t + \Delta t/2) = \mathbf{p}(t - \Delta t/2) + \Delta t \mathbf{F}\left(\mathbf{r}(t)\right) + O\left(\Delta t^3\right) \\ \mathbf{r}(t + \Delta t) = \mathbf{r}(t) + \mathbf{p}(t + \Delta t/2) + O\left(\Delta t^3\right) \end{cases} \tag{2.35}$$

which has the following map:

$$\begin{cases} \mathbf{p}_{n+1/2} = \mathbf{p}_{n-1/2} + \Delta t \mathbf{F}(\mathbf{r}_n) \\ \mathbf{r}_{n+1} = \mathbf{r}_n + \mathbf{p}_{n+1/2} \frac{\Delta t}{2} \end{cases} \tag{2.36}$$

(as always, for simplicity we keep $m_{\text{mass}} = q_{\text{charge}} = 1$).

For integer time, the momentum is this:

$$\mathbf{p}_n = \frac{\mathbf{p}_{n-1/2} + \mathbf{p}_{n+1/2}}{2} \tag{2.37}$$

remembering that we're doing an error of the order $O\left(\Delta t^2\right)$

If we consider a relativistic case, the map is modified as follows:

$$\begin{cases} \mathbf{p}_{n+1/2} = \mathbf{p}_{n-1/2} + \Delta t \mathbf{F}(\mathbf{r}_n) \\ \mathbf{r}_{n+1} = \mathbf{r}_n + \frac{\Delta t}{2} \frac{\mathbf{p}_{n+1/2}}{\gamma_{n+1/2}} \end{cases} \tag{2.38}$$

in which $\mathbf{F}_n = \mathbf{E}_n + \frac{\mathbf{p}_n}{\gamma_n} \times \mathbf{B}_n$ so that

$$\begin{cases} \mathbf{p}_{n+1/2} = \mathbf{p}_{n-1/2} + \Delta t \left(\mathbf{E}_n + \frac{\mathbf{p}_{n-1/2} + \mathbf{p}_{n+1/2}}{2\gamma_n} \times \mathbf{B}_n \right) \\ \mathbf{r}_{n+1} = \mathbf{r}_n + \frac{\Delta t}{2} \frac{\mathbf{p}_{n+1/2}}{\gamma_{n+1/2}} \end{cases} \tag{2.39}$$

To solve the implicit equation for $\mathbf{p}_{n\pm1/2}$, instead of using 2.37, we can write $\mathbf{p}_n$ as a half-step advancement over $\mathbf{p}_{n-1/2}$, obtaining a new but simpler implicit equation:

$$\mathbf{p}_n = \mathbf{p}_{n-1/2} + \frac{\Delta t}{2} \left(\mathbf{E}_n + \frac{\mathbf{p}_n}{\gamma_n} \times \mathbf{B}_n \right) \tag{2.40}$$

Setting:

$$\begin{aligned} \beta &= \Delta t/2 \\ \mathbf{p}_* &= \mathbf{p}_{n-1/2} + \beta \mathbf{E}_n \\ \mathbf{b} &= \beta \mathbf{B}_n / \gamma_n \end{aligned} \tag{2.41}$$

equation 2.40 can be rewritten in this way:

$$\mathbf{p}_n = \mathbf{p}_* + \mathbf{p}_n \times \mathbf{b} \tag{2.42}$$

or also:

$$\mathbf{p}_* = \mathbf{p}_n - \mathbf{p}_n \times \mathbf{b} \tag{2.43}$$

$$\mathbf{p}_n \times \mathbf{b} = \mathbf{p}_n - \mathbf{p}_* \tag{2.44}$$

Multiplying on the right $\times\mathbf{b}$ the 2.43

$$\mathbf{p}_* \times \mathbf{b} = \mathbf{p}_n \times \mathbf{b} - (\mathbf{p}_n \times \mathbf{b}) \times \mathbf{b} \tag{2.45}$$

Using the vector identity

$$\mathbf{C} \times (\mathbf{B} \times \mathbf{A}) = \mathbf{A} \times (\mathbf{B} \times \mathbf{C}) = \mathbf{B}(\mathbf{A} \cdot \mathbf{C}) - \mathbf{C}(\mathbf{A} \cdot \mathbf{B})$$

we can rewrite the $(\mathbf{p}_n \times \mathbf{b}) \times \mathbf{b}$ term as

$$\begin{aligned}(\mathbf{p}_n \times \mathbf{b}) \times \mathbf{b} &= \mathbf{b} \times (\mathbf{p}_n \times \mathbf{b}) = \mathbf{p}_n(\mathbf{b} \cdot \mathbf{b}) - \mathbf{b}(\mathbf{b} \cdot \mathbf{p}_n) = \\ &= \mathbf{p}_n\mathbf{b}^2 - \mathbf{b}(\mathbf{b} \cdot \mathbf{p}_n)\end{aligned} \tag{2.46}$$

If we multiply the 2.43 by $\cdot\mathbf{b}$ on the right we get

$$\mathbf{p}_* \cdot \mathbf{b} = \mathbf{p}_n \cdot \mathbf{b} - \underbrace{(\mathbf{p}_n \times \mathbf{b}) \cdot \mathbf{b}}_{\text{it's 0 by definition}} \tag{2.47}$$

so that

$$\mathbf{p}_* \cdot \mathbf{b} = \mathbf{p}_n \cdot \mathbf{b} \tag{2.48}$$

Combining 2.46 with 2.48 we get

$$\mathbf{b} \times (\mathbf{p}_n \times \mathbf{b}) = \mathbf{p}_n\mathbf{b}^2 - \mathbf{b}(\mathbf{b} \cdot \mathbf{p}_*)$$

$$\mathbf{p}_n\mathbf{b}^2 = \mathbf{b} \times (\mathbf{p}_n \times \mathbf{b}) + \mathbf{b}(\mathbf{b} \cdot \mathbf{p}_*)$$

Using 2.44 we get

$$\begin{aligned}\mathbf{b}^2\mathbf{p}_n &= \mathbf{b} \times (\mathbf{p}_n - \mathbf{p}_*) + \mathbf{b}(\mathbf{b} \cdot \mathbf{p}_*) \\ \mathbf{b}^2\mathbf{p}_n &- \mathbf{b} \times \mathbf{p}_n = -\mathbf{b} \times \mathbf{p}_* + \mathbf{b}(\mathbf{b} \cdot \mathbf{p}_*) \\ \mathbf{b}^2\mathbf{p}_n &+ \mathbf{p}_n \times \mathbf{b} = \mathbf{p}_* \times \mathbf{b} + \mathbf{b}(\mathbf{b} \cdot \mathbf{p}_*)\end{aligned}$$

Applying 2.44 again it becomes

$$\begin{aligned}\mathbf{b}^2\mathbf{p}_n + \mathbf{p}_n - \mathbf{p}_* &= \mathbf{p}_* \times \mathbf{b} + \mathbf{b}(\mathbf{b} \cdot \mathbf{p}_*) \\ \mathbf{p}_n(\mathbf{b}^2 + 1) &= \mathbf{p}_* + \mathbf{p}_* \times \mathbf{b} + \mathbf{b}(\mathbf{b} \cdot \mathbf{p}_*)\end{aligned}$$

and finally

$$\mathbf{p}_n = \frac{1}{\mathbf{b}^2 + 1}\left[\mathbf{p}_* + \mathbf{p}_* \times \mathbf{b} + \mathbf{b}(\mathbf{b} \cdot \mathbf{p}_*)\right] \tag{2.49}$$

To solve 2.40 we are more interested in $\mathbf{p}_n \times \mathbf{b}$. So let's multiply 2.49 $\times\mathbf{b}$:

$$\mathbf{p}_n \times \mathbf{b} = \frac{1}{\mathbf{b}^2 + 1}\left[\mathbf{p}_* + \mathbf{p}_* \times \mathbf{b}\right] \times \mathbf{b} \tag{2.50}$$

Inserting 2.50 in 2.39 gives the final expression for the second order leapfrog algorithm:

$$\mathbf{p}_{n+1/2} = \mathbf{p}_{n-1/2} + \Delta t \mathbf{E}_n + \frac{1}{\mathbf{b}^2 + 1} \left(\mathbf{p}_* + \mathbf{p}_* \times \mathbf{b} \right) \times \mathbf{b} \tag{2.51}$$

Thanks to 2.41,

$$2\mathbf{p}_* = 2\mathbf{p}_{n-1/2} + \Delta t \mathbf{E}_n \longrightarrow \mathbf{p}_{n-1/2} + \Delta t \mathbf{E}_n = 2\mathbf{p}_* - \mathbf{p}_{n-1/2}$$

so that we can write the whole solution in terms of $\mathbf{p}_{n-1/2}$ and $\mathbf{p}_*$, which are known:

$$\mathbf{p}_{n+1/2} = 2\mathbf{p}_* - \mathbf{p}_{n-1/2} + \frac{1}{\mathbf{b}^2 + 1} \left(\mathbf{p}_* + \mathbf{p}_* \times \mathbf{b} \right) \times \mathbf{b} \tag{2.52}$$

Of course, we could have done similar calculations with an inverse leapfrog:

$$\begin{cases} \mathbf{r}_{n+1/2} = \mathbf{r}_{n-1/2} + \Delta t \frac{\mathbf{p}_n}{\gamma_n} \\ \mathbf{p}_{n+1} = \mathbf{p}_n + \Delta t \mathbf{F}(\mathbf{r}_{n+1/2}) \end{cases} \tag{2.53}$$

2.3.2 Fourth order scheme (LF4)

This scheme is composed of three inverse leapfrog maps: given the weight

$$\alpha = \frac{1}{2 - 2^{1/3}} \tag{2.54}$$

we define the following algorithm.

First part

$$\Delta t_x = \alpha \Delta t \qquad\qquad \Delta t_p = \alpha \Delta t$$

$$\text{Map } M_1 = \begin{cases} \mathbf{r}_{n+\alpha/2} = \mathbf{r}_{n-\alpha/2} + \Delta t_x \mathbf{v}_n \\ \mathbf{p}_{n+\alpha} = \mathbf{p}_n + \Delta t_p \mathbf{F}(\mathbf{r}_{n+\alpha/2}, \mathbf{v}_{n+\alpha/2}, t_n + \Delta t_p/2) \\ t_{n,(1)} = t_n + \Delta t_p \end{cases} \tag{2.55}$$

in which $\mathbf{p}_{n+\alpha/2} = \left(\mathbf{p}_n + \mathbf{p}_{n+\alpha} \right)/2$.

Second part

$$\Delta t_x = \frac{1-\alpha}{2}\Delta t \qquad\qquad \Delta t_p = (1-2\alpha)\Delta t$$

$$\text{Map } M_2 = \begin{cases} \mathbf{r}_{n+1/2} = \mathbf{r}_{n+\alpha/2} + \Delta t_x \mathbf{v}_{n+\alpha} \\ \mathbf{p}_{n+1-\alpha} = \mathbf{p}_{n+\alpha} + \Delta t_p \mathbf{F}(\mathbf{r}_{n+1/2}, \mathbf{v}_{n+1/2}, t_{n,(1)} + \Delta t_p/2) \\ t_{n,(1)} = t_{n,(1)} + \Delta t_p \end{cases} \tag{2.56}$$

in which $\mathbf{p}_{n+1/2} = (\mathbf{p}_{n+1-\alpha} + \mathbf{p}_{n+\alpha})/2$

Third part

$$\Delta t_x = \frac{1-\alpha}{2}\Delta t \qquad\qquad \Delta t_p = \alpha \Delta t$$

$$\text{Map } M_3 = \begin{cases} \mathbf{r}_{n+1-\alpha/2} = \mathbf{r}_{n+1/2} + \Delta t_x \mathbf{v}_{n+1-\alpha} \\ \mathbf{p}_{n+1} = \mathbf{p}_{n+1-\alpha} + \Delta t_p \mathbf{F}(\mathbf{r}_{n+1-\alpha/2}, \mathbf{v}_{n+1-\alpha/2}, t_{n,(2)} + \Delta t_p/2) \\ t_{n,(3)} = t_{n,(2)} + \Delta t_p \end{cases} \tag{2.57}$$

in which $\mathbf{p}_{n+1-\alpha/2} = (\mathbf{p}_{n+1} + \mathbf{p}_{n+1-\alpha})/2$

It's easy to see that

$$t_{n,(3)} = t_{n+1} = t_n + \Delta t \tag{2.58}$$

and that

$$\begin{pmatrix} \mathbf{r}_{n+1-\alpha/2} \\ \mathbf{p}_{n+1} \end{pmatrix} = M_3 \circ M_2 \circ M_1 \begin{pmatrix} \mathbf{r}_{n-\alpha/2} \\ \mathbf{p}_n \end{pmatrix} \tag{2.59}$$

The step advancement is completed with

$$\mathbf{r}_{n+1} = \mathbf{r}_{n+1-\alpha/2} + \frac{\alpha \Delta t}{2}\mathbf{v}_{n+1} \tag{2.60}$$

2.4 PICcol: my code to compare integrators in a PIC environment

It's should be easy to understand that calculating Coulomb interactions between every particle pair in a plasma can be a really nightmare also for a supercomputer. One simple approximation that is always used is based on discretization: we can consider the charges as a source of a field, that we calculate only at some fixed points. Then the particles themselves interacts with this field and not between them. This is the grid used in a Particle In Cell

(PIC) software. Also, to reduce the number of the particles but to preserve the other characteristics, we can use *macroparticles*, so that each *object* in the software represents many elementary protons (or ions), with their mass and charge summed.

Unfortunately, those approximations do not accurately reproduce the microscopic dynamics of plasma. But we have to understand that, first of all, we are more interested in the accuracy of collective plasma phenomena and less in the accuracy of individual particle orbits. But do such errors modify the macroscopic behaviour? We could say yes. The primary source of error can be identified in the limited dimensionality of our simulations: doing a full $3D$ simulation, even with all those approximations, with a meaningful number of particles and a reasonable accuracy, is still unfeasible. Doing a $2D$ simulation, on the other hand, destroys many plasma properties, such as the value of the charge. There're some methods to infer them, but they are subject to other errors and approximations (such as hypothesizing cylindrical symmetry). Also, there're usually far too few particles (causing exaggeration of fluctuations and collisions), there're serious problems with initial and boundary conditions, round-off errors and many other difficult to assess in practice [24].

Anyway, I wrote a small PIC code to analyse differences in integrators. The code can also work without any grid and so in principle it could also verify errors introduced by this approximation (those graphs are not described in this thesis).

INPUT

At time $t = 0$ the software needs in input this data:

- Number of particles
- System size
- Number of grid points
- Particles position and velocity
- **E** and **B** values on the grid

PROCESSING

- Field values have to be ported from grid to particles
  - $E_{i,j,k} \rightarrow E(x_p)$
  - $B_{i,j,k} \rightarrow B(x_p)$
- LEAPFROG

  - $p^{n+1/2} = p^{n-1/2} + \Delta t \left[E^n + v^n \times B^n\right]$
  - $x^{n+1} = x^n + \Delta t \cdot v^{n+1/2}$
  - The speed $v^n = p^n/\gamma^n$ can be calculated defining the mean

$$p^n = \left(p^{n+1/2} + p^{n-1/2}\right)/2$$

    We find ourselves with an implicit equation that can be calculated explicitly with this method
  - $p^n = p^{n-1/2} + \beta \left[E^n + (p^n/\gamma^n) \times B\right]$
    $\rightarrow\ p^n = p^* + p^n \times b$ where $p^* = p^{n-1/2} + \beta E^n$ and $b = \beta B^n/\gamma^n$
    $\rightarrow\ p^n - p^n \times b = p^*$ we multiply each term on the right with $\times b$
    $\rightarrow\ p^n \times b - (p^n \times b) \times b = p^* \times b$
    $\rightarrow\ p^n = \left(1 + b^2\right)^{-1} \left[p^* + p^* \times b + b(p^* \cdot b)\right]$
  - $p^{n+1/2} = 2p^n - p^{n-1/2}$
  - $x^{n+1} = x^n + \Delta t \cdot v^{n+1/2}$

- From values x^n, x^{n+1}, $v^{n+1/2}$ summing on each and every species, I have to find the currents on grid points $(J_{i,j,k})$
- Fields evolution $(E^n, B^n) \rightarrow \left(E^{n+1}, B^{n+1}\right)$
  - $B^n = B^{n-1/2} - \frac{1}{2}\Delta t \nabla \times E^n$
  - $B^{n+1/2} = B^n - \frac{1}{2}\Delta t \nabla \times E^n$
  - $E^{n+1} = E^n + \Delta t \left[\nabla \times B^{n+1/2} - J^{n+1/2}\right]$
  - $B^{n+1} = B^{n+1/2} - \Delta t \nabla \times E^{n+1}$

OUTPUT

As we can see from figures 2.5, 2.6 and 2.7, we can say that a 2^{nd} order leapfrog algorithm is substantially similar to a symplectic integrator.

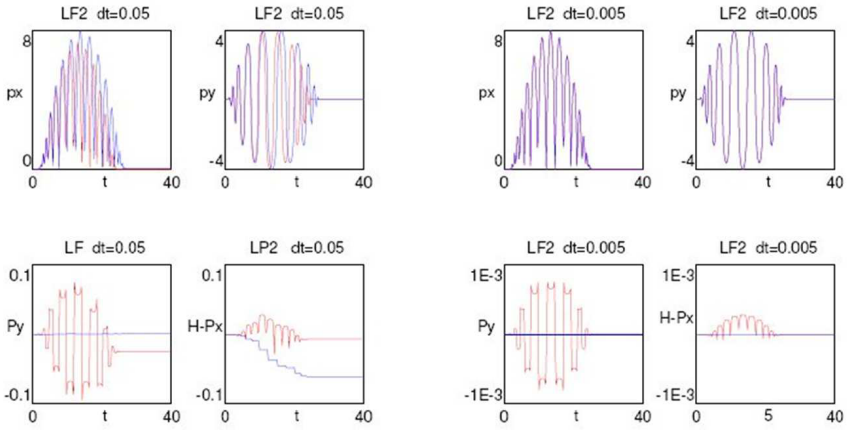

Figure 2.5: *Leapfrog 2^{nd} order (red) vs Runge-Kutta 4^{th} order (blue) for prime integrals, p_x, p_y, P_y and $H - P_x$.*

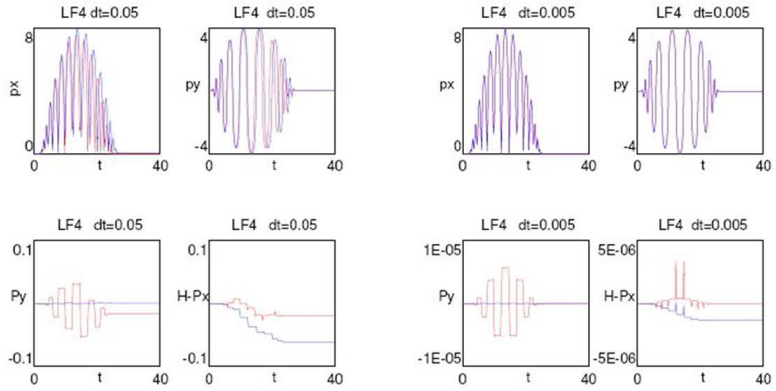

Figure 2.6: *Leapfrog 4^{th} order (red) vs Runge-Kutta 4^{th} order (blue) for prime integrals, p_x, p_y, P_y and $H - P_x$.*

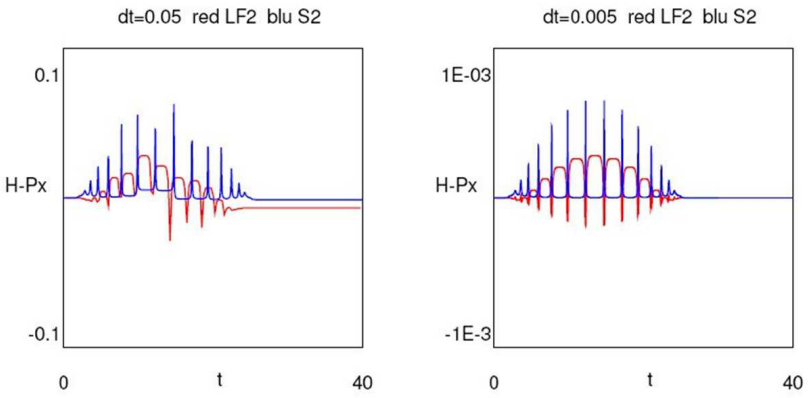

Figure 2.7: *Leapfrog 2^{nd} order (red) vs symplectic 2^{nd} order (blue) for prime integrals, p_x, p_y, P_y and $H - P_x$.*

CHAPTER 3

Protons transport

The main problem studied within this thesis is the transport of the protons obtained from laser-plasma interactions.

This kind of problem is still an open question within the physics community: it's really complex and we're still trying to understand which devices should be the best for this task. To make accelerated protons useful, in fact, we need to carry them away from the target zone: we cannot install a post-acceleration device so close to the interaction point (and also the bunch would not be good enough at this point) and, for example, we couldn't even ask for a patient that requires a proton-therapy to stay within this region with gas jets and powerful electromagnetic devices.

So, we must be able to transport these bunches for at least a few dozens of centimeters. What could we use? In this chapter I will describe how we started looking at classical FODO beamlines (focusing-defocusing quadrupoles) and how we then arrived to the solenoid, based on the experience that other groups made on this topic.

This study has been done using a code developed and extended by me during the period of my thesis. It's able to track particles independently when propagating along a beamline composed of different magnetic elements. The newest version, written in `C++`, is parallelized and uses some strictly defined interfaces to read input and write the simulations to disk, so that it can work in the environment built with all the other codes of the group.

3.1 Transport of protons coming from TNSA regime

The main characteristic of an optically accelerated beam, in TNSA regime, is its exponential spectrum of energy, with a cutoff $E_{max}(\infty)$ [25]. What it's really interesting is not the upper cutoff $E_{\max}(\infty)$, but the mean energy. For the injection it's important that the beam is almost monochromatic, but at the highest energies the intensities are really low. In fact

$$\rho(E) = \frac{dN}{dE} = \frac{E_0}{N_0} e^{-E/E_0} \vartheta \left(E_{\max}(\infty) - E\right) \tag{3.1}$$

If we suppose that $E_{\max}(\infty) \gg \langle E \rangle$, the upper cut can be ignored and we immediately verify that the total number of particles is given by

$$N_{\text{tot}} = \int_0^\infty \frac{dN}{dE} dE = N_0 \int_0^\infty e^{-u} du = N_0 \tag{3.2}$$

Analogously, the total energy is:

$$E_{\text{tot}} = \int_0^\infty E \frac{dN}{dE} dE = N_0 \; E_0 \int_0^\infty u \; e^{-u} du = N_0 \; E_0 \tag{3.3}$$

The mean energy can be expressed as:

$$\langle E \rangle = \frac{E_{\text{tot}}}{N_{\text{tot}}} = E_0 \tag{3.4}$$

The number of particles in a small interval $[E, E + \Delta E]$ is

$$N\left([E, E + \Delta E]\right) = \int_E^{E+\Delta E} E \frac{dN}{dE} dE = N_0 \int_{E/E_0}^{(E+\Delta E)/E_0} e^{-u} du \simeq N_0 \frac{\Delta E}{E_0} e^{-E/E_0} \tag{3.5}$$

Let's suppose that we want to select protons with an energy of $E = 10$ MeV and a spread of 0.1 MeV, or 1%. Under these conditions the fraction $n(E_0) = N(E_0)/N_0$ of protons at different E_0 mean energies is

$$n(2) = 6.7 \; 10^{-5} \quad n(2.5) = 1.8 \; 10^{-4} \quad n(3) = 3.6 \; 10^{-4}$$

$$n(4) = 8.2 \; 10^{-4} \quad n(5) = 1.3 \; 10^{-3}$$

We clearly see that if we start from $N_0 = 10^{11}$ protons we need to have a mean energy that is between 2.5 and 5 MeV, to have a minimum of 10^7 injectable protons, keeping under consideration also the transport beamline and its losses.

There are two main types of target: solid targets and liquid hydrogen. From simulations [26] it's clear that the mean energy is greater for liquid hydrogen: the percentage of the laser energy converted into kinetic energy of protons reaches 10%.

We can estimate the number of protons that are accelerated knowing their mean energy and the energy in a laser pulse. For example, at the Dresden-Rossendorf (ZFD) research centre [27], the laser *DRACO* has an energy of 3 J and the mean energy of the protons ejected is 2 MeV: considering previous results, the transferred energy so is approximately 0.3 J and the number of protons that we get is

$$N_0 = \frac{0.1\ E_{\text{laser}}}{E_0} = \frac{0.3\ \text{J}}{2\ \text{MeV}} = \frac{0.3\ \text{J}}{2 \times 1.6\ 10^{-13}\ \text{J}} \sim 10^{13}$$

Their data give us this numbers for the accelerated protons distribution:

$$\frac{dN}{dE\ d\Omega} = 3\ 10^{11}\ e^{-E/E_0}\ \text{MeV}^{-1} \qquad E_0 = 1.7\ \text{MeV} \tag{3.6}$$

Unfortunately, they do not describe the angular distribution. If we assume it as uniform in the forward direction (angle = 2π), we have

$$N_0 = 1.7 \times 2\pi \times 3\ 10^{11} = 3\ 10^{12} \tag{3.7}$$

If we consider a cone obtained with a collimator (iris) with $|\phi| \leq 0.1$ rad, that corresponds to an aperture of $2 \times 0.1 \times 180/\pi = 0.2$ rad $\sim 11°$, the number of protons that we get according to Eq. 3.7 is $N = 1.7 \times 0.2 \times 3\ 10^{11} \sim 10^{11}$. The number of protons with an energy of 10.0 ± 0.1 MeV is $2.6\ 10^7$. We are within the limits, but with a strict margin. We have to consider that a uniform angular distribution means that only the 3% of the laser energy is converted, instead of the commonly accepted 10%. So it's possible that the energy transfer is less efficient for *DRACO*, that the spectrum underestimates the real values or that the energy distribution is not uniform in angle.

3.2 Lilia and Prometheus

Our group works within the *Lilia* collaboration, aimed to simulate and do feasibility studies for the Flame laser at LNF (Frascati) [28], studying new gaseous targets and transport lines. We are also doing some feasibility studies for a new facility, *Prometheus*, based on a high power laser, aimed to have proton bunches for biomedical studies and applications. This project is done in collaboration with the ENEA division in Bologna and some other private funds.

Lilia experiment aims to obtain significant advances in the knowledge of physical phenomena regarding laser-accelerated proton bunches. The objective is to get a beam with protons of at least 50 MeV of energy and intensity in the order of 10^{13}. To reach this target, many activities will be done regarding theoretical studies of laser-plasma interactions and new regimes of accelerations, experimental studies of target configurations, focusing devices and new kinds of detectors to analyse the beam obtained.

3.3 My experience at the Goethe University in Frankfurt

To do part of the work I went to the Frankfurt Goethe University. I worked there for six weeks and my tasks were supposed to be mainly focused on the code check: in Bologna I worked on developing a new code, *Propaga*, started by Prof. Servizi, that tracks particles propagating along a beamline.

Just few days before my departure, with Prof. G. Servizi we developed a tool to animate simulated particles. It took a couple of days while I was in Frankfurt to make the program working in a portable way. Previously, films were not reproducible on a machine different from the original creator and so I was not able to play them remotely.

After having fixed those problems, I went on comparing our results with LORASR and Trace-3D ones [29, 30]. Those are *trusted* codes that are used to design cavities and so they are a great opportunity to find and fix any problem that could arise in our simulations. The first software, in particular, belongs to the University of Frankfurt.

One way to do these first checks is to compare beam envelopes. Immediately, I discovered that I couldn't get those graphs from our simulations, so I wrote a small tool to gather that data from our output and while I was developing it I also added the possibility to track one single custom defined particle along the whole beamline.

Using

$$\begin{aligned}
\sigma_x &= \langle x^2 \rangle - \langle x \rangle \langle x \rangle \\
\sigma_y &= \langle y^2 \rangle - \langle y \rangle \langle y \rangle \\
\sigma_z &= \langle z^2 \rangle - \langle z \rangle \langle z \rangle \\
\sigma_{p_x} &= \langle p_x^2 \rangle - \langle p_x \rangle \langle p_x \rangle \\
\sigma_{p_y} &= \langle p_y^2 \rangle - \langle p_y \rangle \langle p_y \rangle \\
\sigma_{p_z} &= \langle p_z^2 \rangle - \langle p_z \rangle \langle p_z \rangle \\
m_x &= \langle x p_x \rangle - \langle x \rangle \langle p_x \rangle \\
m_y &= \langle y p_y \rangle - \langle y \rangle \langle p_y \rangle \\
m_z &= \langle z p_z \rangle - \langle z \rangle \langle p_z \rangle
\end{aligned}$$

we defined emittances in this way:

$$\begin{aligned}
\epsilon_x &= \sqrt{\sigma_x \, \sigma_{p_x} - m_x^2} \\
\epsilon_y &= \sqrt{\sigma_y \, \sigma_{p_y} - m_y^2} \\
\epsilon_z &= \sqrt{\sigma_z \, \sigma_{p_z} - m_z^2}
\end{aligned} \tag{3.8}$$

3.3.1 BuGe: my bunch generator

In the beginning, when we started the checking of the code, we decided to use a uniform distribution for the input bunch and not one of the *realistic* bunches that I had, produced by ALaDyn. In this way, bunches are better defined and their properties are completely under our control. But this also means that a bunch generator is needed, and so I wrote one from scratch recycling some number generator routines from previous works.

This work required a lot of time, because I had to learn particle distributions, in particular the Kapchinskij-Vladimirskij one.

Kapchinskij-Vladimirskij distribution

In a paper presented in the International Conference on High-Energy Accelerators and Instrumentation at CERN in 1959, I. M. Kapchinskij and V. V. Vladimirskij discussed the space charge significance to the beam cross-section in the stationary conditions for a definite phase volume of injected particles [31, 32].

They made the following assumptions when deducing their phase-space distributions of particles:

- the beam cross-section is appreciably smaller than the variation period of the focusing field;
- the particles move only in the linear region of the external field close to the accelerator's axis;
- the influence of the space charge is essential only at relatively small velocities, so that it is assumed that the particle velocity is much below the velocity of light;
- the energy increment in a gap is sufficiently small, so that the period of synchrotron oscillations is much greater than the acceleration period.

In these assumptions, the equations of transversal oscillations for a particle propagating into magnetic quadrupole lenses may be expressed in the following form

$$\frac{d^2x}{d\tau^2} + Q_x(\tau)\cdot x + \frac{e\lambda^2}{mc^2}\cdot\frac{\partial U_K}{\partial x} = 0 \tag{3.9}$$

$$\frac{d^2y}{d\tau^2} + Q_y(\tau)\cdot y + \frac{e\lambda^2}{mc^2}\cdot\frac{\partial U_K}{\partial y} = 0 \tag{3.10}$$

$$\tag{3.11}$$

where z is directed along the axis of the accelerator. The independent variable τ is defined as

$$\tau = \frac{ct}{\lambda}$$

and

- e, m are charge and mass of the particle;
- λ is the wavelength of the high frequency accelerating field in free space;
- $U_K(x, y, z)$ is the potential of the field of the beam space charge.
- $Q_x(\tau) = Q_1(\tau) + Q_2(\tau)$;
- $Q_x(\tau) = Q_1(\tau) - Q_2(\tau)$;

where the functions $Q_1(\tau)$ is the defocusing action of the accelerating gaps and $Q_2(\tau)$ is determined by the focusing field:

$$Q_1(\tau) = \frac{e\lambda^2}{2mc^2} \cdot \frac{\partial E_z(r, z, \tau)}{\partial z}$$
$$Q_2(\tau) = \lambda^2 \frac{e\beta}{mc^2} \cdot G \cdot g(\tau)$$

$g(\tau)$ has the period of the focusing field and changes within the limits $|g(\tau)| \leq 1$, G is the magnetic field gradient on the axis in the middle portion of the lens.

The period of the beam cross-section change has the same value order as the period of the focusing field; since the beam cross-section is substantially smaller than the period of cross-section changes, the field of the space charge $\mathbf{E}_k$ changes much slower along the axis z than along the axes x and y:

$$\left|\frac{\partial E_{kz}}{\partial z}\right| \ll \left|\frac{\partial E_{xk}}{\partial x}\right|, \left|\frac{\partial E_{yk}}{\partial y}\right|$$

Thus

$$\mathrm{div}\mathbf{E} \approx \frac{\partial E_{xk}}{\partial x} + \frac{\partial E_{yk}}{\partial y}$$

from which

$$\frac{\partial^2 U_K}{\partial x^2} + \frac{\partial^2 U_K}{\partial y^2} = -4\pi \cdot \rho(x, y, z) \tag{3.12}$$

Let's assume that $n(x, y, z, \dot{x}, \dot{y}, \dot{z})$ is the density of particle distribution in the phase space of coordinates and velocities. According to Liouville's theorem, the function n remains constant along the trajectory of the particle motion in the phase space, so that n depends only on the integrals of motion.

The space charge density in the beam $\rho(x, y, z)$ is determined by the integral

$$\rho(x, y, z) = e \iiint n(x, y, z, \dot{x}, \dot{y}, \dot{z})\, d\dot{x}d\dot{y}d\dot{z} \tag{3.13}$$

The equations 3.9 and 3.10 should be solved jointly with equations 3.12 and 3.13, which determine the potential of the space charge field $U_K(x, y, z)$, provided the phase density of particles n is a function of the integrals of motion of equations 3.9 and 3.10.

The integration of equations 3.9 and 3.10 will be materially simplified if we introduce a special assumption regarding the law of particle distribution in the phase space; namely, if we choose such a dependence of phase density upon the integrals of motion so that they become linear in the separated variables.

Let's consider equation 3.9; if it's linear regarding to the function $x(\tau)$, then it's possible to choose a pair of complex-conjugated fundamental solutions

$$\chi_x(\tau) = \delta_x(\tau)\ e^{i\psi_x(\tau)}$$
$$\chi_x^*(\tau) = \delta_x(\tau)\ e^{-i\psi_x(\tau)}$$

which make it possible to express any real solution with arbitrary initial conditions as

$$x(\tau) = A_x \cdot \delta_x(\tau)\ \cos\left[\psi_x(\tau) + \theta_x\right] \tag{3.14}$$

The Wronskian of the functions χ_x and χ_x^*, which is defined as

$$W(f_1, f_2)(x) = \det \begin{vmatrix} f_1(x) & f_2(x) \\ f_1'(x) & f_2'(x) \end{vmatrix}$$

is a well known constant value. Let's put

$$\chi_x \frac{d\chi_x^*}{d\tau} - \chi_x^* \frac{d\chi_x}{d\tau} = -2i \tag{3.15}$$

It follows from 3.15 that

$$\frac{d\psi_x}{d\tau} = \frac{1}{\delta_x^2}$$

The solution of the equation 3.10 has the analogous form

$$y(\tau) = A_y \cdot \delta_y(\tau)\ \cos\left[\psi_y(\tau) + \theta_y\right]$$
$$\frac{d\psi_y}{d\tau} = \frac{1}{\delta_y^2} \tag{3.16}$$

The values A_x, A_y, θ_x, θ_y depend only upon the initial conditions and consequently are the integrals of motion. The phases of the transversal oscillations of particles θ_x, θ_y are cyclic functions of the initial coordinates and velocities. It's natural to suppose that the function of density distribution n depends only upon the integrals of motion A_x, A_y which are characteristic of the transversal oscillation intensity. The oscillation phases θ_x, θ_y may be of arbitrary value. We shall obtain the expressions for the integrals A_x and A_y by eliminating from the functions $(x(\tau), dx/d\tau)$ and $(y(\tau), dy/d\tau)$ the phases (θ_x, θ_y):

$$\left(\delta_x \dot{x} - \dot{\delta}_x x\right)^2 + \left(\frac{x}{\delta_x}\right)^2 = A_x^2$$
$$\left(\delta_y \dot{y} - \dot{\delta}_y y\right)^2 + \left(\frac{y}{\delta_y}\right)^2 = A_y^2$$

Let's now assume that the particle distribution density in phase space depends upon the integrals of motion in the following way:

$$n = n_0 \, \delta(F - F_0)$$

where in a general case

$$F = A_x^2 + s \, A_y^2$$

and δ is the usual δ-function. We shall assume further on that $s = 1$, so we get

$$F = A_x^2 + A_y^2$$

Thus, due to the assumption, all the particles in a four-dimensional phase-space x, y, $\dot{x}$, $\dot{y}$ are situated on the surface of the ellipsoid

$$\left(\delta_x \dot{x} - \dot{\delta}_x x\right)^2 + \left(\frac{x}{\delta_x}\right)^2 + \left(\delta_y \dot{y} - \dot{\delta}_y y\right)^2 + \left(\frac{y}{\delta_y}\right)^2 = F$$

The projections of the representing points on the plane x, $\dot{x}$, y, $\dot{y}$ fill up the corresponding ellipses

$$\left(\delta_x \dot{x} - \dot{\delta}_x x\right)^2 + \left(\frac{x}{\delta_x}\right)^2 = A_{x,\max}^2$$
$$\left(\delta_y \dot{y} - \dot{\delta}_y y\right)^2 + \left(\frac{y}{\delta_y}\right)^2 = A_{y,\max}^2$$

Code development

Using some defined conditions upon the KV ellipses (Twiss parameters), I built a really simple bunch generator that is able to create uniformly distributed bunches in each dimension (x, y, z, p_x, p_y, p_z).

$$\frac{x^2}{R^2} + \frac{x'^2}{\theta^2} + \frac{y^2}{R^2} + \frac{y'^2}{\theta^2} = 1 \tag{3.17}$$

where θ is the opening angle and R is the maximum beam radius (in x and y).

Of course, the code implementation differs a little from this equation, mainly because I accepted not only the real surface of the ellipsoid but a region that is between 0.95 and 1.00. Imposing the equality to 1 would have meant to reject most of the particles generated by our Monte-Carlo number generator, while accepting a *skin* larger than 0.05 could cause bad effects because the projections would have not been uniform again.

With these conditions, the plots of the coordinates of the generated particles became acceptable. In figures [3.1 and 3.2] there's an example of a uniformly distributed bunch, made with these parameters:

- bunch radius: 60 nm
- bunch length: 22 nm
- average energy: $\sim$ 10.1 MeV
- energy spread: $\sim$ 6 %

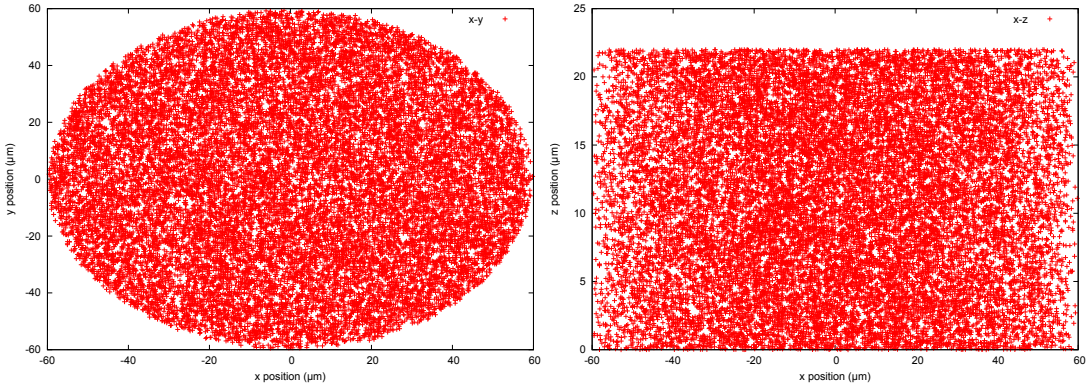

Figure 3.1: *On the left, xy distribution of uniformly generated particles; on the right, the xz distribution.*

3.4 Propaga

3.4.1 Introduction to our code

Our group in Bologna developed a code for particle tracking along a beamline. Its name is *Propaga*. It was written quickly, but with the intention to create a good software and not to replace it very soon.

When I arrived in Frankfurt in June of this year, the status of the code development was considered good: it was able to track particles along many types of magnetic element, like

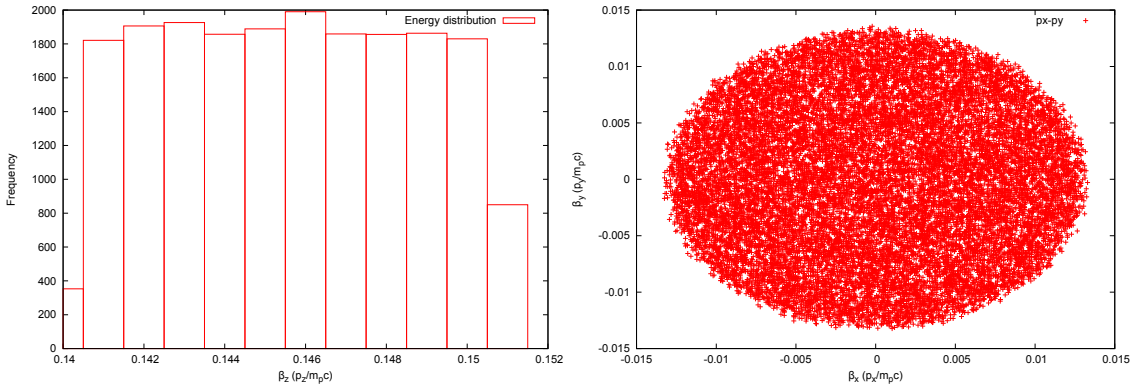

Figure 3.2: *On the left, energy distribution of uniformly generated particles; on the right, transverse momentum (β_x and β_y)*

quadrupoles (focusing and defocusing) and solenoids. It lacked, and still lacks, any kind of space-charge effects treatment and RF cavities.

To begin the checks of our code, I compared it with some simulations done with ASTRA, a tool from DESY that I started learning before leaving to Frankfurt [33, 34].

The first test was based on the PHELIX [35] configuration: a really simple beamline with a solenoid with a length of 72 mm placed 15 mm after the target. Because our solenoid used an hard edge approximation, we chose a B-field of 17.8 T, a field that should be enough to focus a bunch with a reference energy of 10.1 MeV $\pm 6\%$ and an opening angle of 90 mrad, which describes approximately the *strength* of the real solenoid.

As you can see from the picture 3.3, we were in good agreement when comparing with ASTRA, used with an input file that asked for an hard edge approximation and that disabled the space-charge effects: the problem is that none of the two software focused the bunch as required, even if our approximation were ignoring defocusing effects like space charges: if wrong, we should have seen more focusing than real, not absence of focus!

So I started analysing deeply how our code works, hoping to find where the problems were, while also studying the subject to understand why ASTRA is failing too.

3.4.2 Maps of the beamline elements

Our code uses a time integration, not a spatial one like most of other tools do. So it was a bit difficult to compare nearly all of the literature with our calculations, because of different approximations and different treatments of the matrices that map each element of a beamline [36, 37].

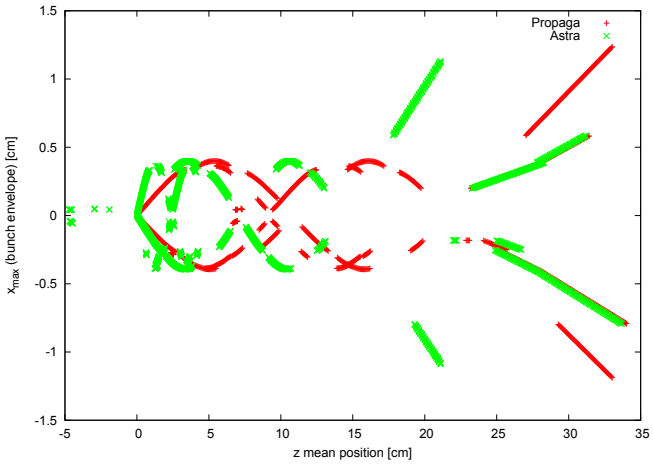

Figure 3.3: *bunch envelope for Astra and Propaga*

Drift map

The map for a drift tube in our code is really easy: velocities are preserved and no forces are applied.

$$\begin{aligned} \frac{dx}{dt} = \dot{x} &= \left(1 + p_x^2 + p_y^2 + p_z^2\right)^{-1/2} p_x = p_x/\gamma \\ \dot{y} &= p_y/\gamma \\ \dot{z} &= p_z/\gamma \\ \dot{p}_x &= 0 \\ \dot{p}_y &= 0 \\ \dot{p}_z &= 0 \end{aligned} \tag{3.18}$$

Focusing quadrupole

Our focusing quadrupole collapses particle on the x-axis.

$$\begin{aligned}
\frac{dx}{dt} = \dot{x} &= \left(1 + p_x^2 + p_y^2 + p_z^2\right)^{-1/2} p_x = p_x/\gamma \\
\dot{y} &= p_y/\gamma \\
\dot{z} &= p_z/\gamma \\
\dot{p}_x &= \frac{qB_0(-\dot{z}x)}{m_p c^2} \\
\dot{p}_y &= \frac{qB_0(\dot{z}y)}{m_p c^2} \\
\dot{p}_z &= \frac{qB_0(\dot{x}x - \dot{y}y)}{m_p c^2}
\end{aligned} \tag{3.19}$$

Defocusing quadrupole

On the other hand, our defocusing quadrupole collapses particle on the y-axis.

$$\begin{aligned}
\frac{dx}{dt} = \dot{x} &= \left(1 + p_x^2 + p_y^2 + p_z^2\right)^{-1/2} p_x = p_x/\gamma \\
\dot{y} &= p_y/\gamma \\
\dot{z} &= p_z/\gamma \\
\dot{p}_x &= \frac{-qB_0(-\dot{z}x)}{m_p c^2} \\
\dot{p}_y &= \frac{-qB_0(\dot{z}y)}{m_p c^2} \\
\dot{p}_z &= \frac{-qB_0(\dot{x}x - \dot{y}y)}{m_p c^2}
\end{aligned} \tag{3.20}$$

Solenoid map

The solenoid was the only device really tested in Frankfurt. At the beginning, the map was only the following:

$$\begin{aligned}
\frac{dx}{dt} = \dot{x} &= \left(1 + p_x^2 + p_y^2 + p_z^2\right)^{-1/2} p_x = p_x/\gamma \\
\dot{y} &= p_y/\gamma \\
\dot{z} &= p_z/\gamma \\
\dot{p}_x &= \frac{qB_0}{m_p c^2} \cdot \frac{p_y}{\gamma} \\
\dot{p}_y &= -\frac{qB_0}{m_p c^2} \cdot \frac{p_x}{\gamma} \\
\dot{p}_z &= 0
\end{aligned} \tag{3.21}$$

But, as we said, with such a map we were not able to describe a focusing effect that we should get with those parameters. After many talks within the group, we found that we were not considering the fringe fields, that describe the curvature of the field lines at the beginning and at the end of the solenoid [38] (Figure 3.4).

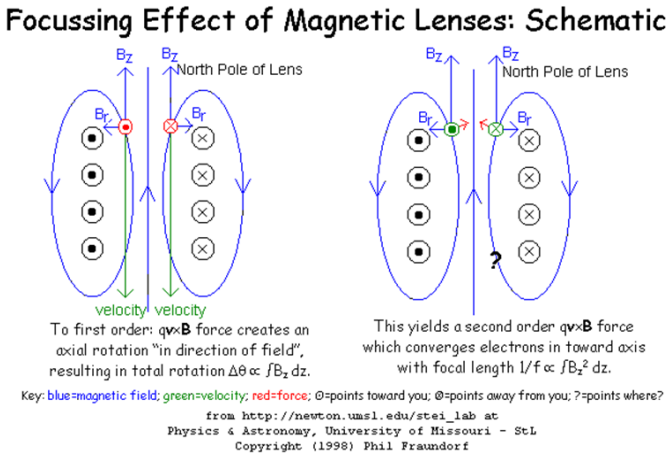

Figure 3.4: *Schematic representation of the focusing effect of a solenoid*

As noted during our discussions, not considering them is not a valid approximation, it means not considering real important physical effects, without them we do not even have any focusing from the solenoid.

Adding them to our software required that I learned it deeply, because it needed some corrections and extensions. In literature, fringe fields matrices are always described as an instant transformation on a space plane and so they do not require any time integration.

But let's look at a more detailed treatment of the fringing fields.

Fringe fields of the solenoid

Defining the potential vector $\mathbf{B} = \nabla \times \mathbf{A}$, owing to the fact that B is defined as constant in the solenoid, we have:

$$\begin{aligned} \oint \mathbf{A} \cdot d\mathbf{l} &= \int B_0 \cdot d\Sigma \\ A\, 2\pi r &= B_0\, \pi r^2 \\ A &= \frac{B_0 \cdot r}{2} \end{aligned} \tag{3.22}$$

Starting from the relativistic Lagrangian

$$\mathcal{L} = -m_0 c^2 \sqrt{1-\beta^2} - e\mathbf{A} \cdot \mathbf{v}$$

the canonical momenta in the transverse plane are defined by

$$\begin{aligned} p_x &= \frac{\partial \mathcal{L}}{\partial \dot{x}} = \gamma m_0 v_x + eA_x \\ p_y &= \frac{\partial \mathcal{L}}{\partial \dot{y}} = \gamma m_0 v_y + eA_y \end{aligned} \tag{3.23}$$

As we know, any magnetic field will not give energy to our particles. So we have to consider angular momentum and energy conservation; owing to the cylindrical symmetry we can write

$$\frac{1}{2}mv_\phi^2 + \frac{1}{2}mv_r^2 + \frac{1}{2}mv_z^2 = \text{const.}$$

for the energy and

$$\mathbf{r} \times \mathbf{p} = r \cdot p_\phi = \text{const.}$$

for the angular momentum. This because

$$\frac{d\mathbf{L}}{dt} = \mathbf{M}_{\text{tot}}$$

where $\mathbf{L}$ is the angular momentum and $\mathbf{M}_{\text{tot}}$ the momentum of the external forces:

$$\mathbf{M}_{\text{tot}} = \mathbf{r} \times \mathbf{F}_{\text{tot}}$$

Because of the fact that the magnetic force is a centripetal force, we have $\mathbf{r} // \mathbf{F}$ and so $\mathbf{M}_{tot} = 0$, that means

$$\frac{d\mathbf{L}}{dt} = 0$$

So let's consider angular momentum conservation: outside (out) the solenoid $A_{\phi,\text{out}} = 0$, inside (in) $A_{\phi,\text{in}} \neq 0$

$$\begin{aligned} r \cdot p_\phi &= \text{const.} \\ mv_{\phi,\text{out}} &= mv_{\phi,\text{in}} + qA_{\phi,\text{in}} = \\ &= mv_{\phi,\text{in}} + \frac{qB_0 \cdot r}{2} \\ mv_{\phi,\text{in}} &= mv_{\phi,\text{out}} - \frac{qB_0 \cdot r}{2} \\ v_{\phi,\text{in}} &= v_{\phi,\text{out}} - \frac{qB_0 \cdot r}{2m} \end{aligned} \tag{3.24}$$

The transformations between the references system are done in this way:

$$\begin{cases} v_x = -v_\phi \cdot \sin\phi \\ v_y = v_\phi \cdot \cos\phi \end{cases}$$

and so

$$\begin{cases} v_{x,\text{in}} = -v_{\phi,\text{in}} \cdot \sin\phi = \left(v_{\phi,\text{out}} - \frac{qB_0 \cdot r}{2m}\right) \cdot \sin\phi = -v_{\phi,\text{out}} \sin\phi + \frac{qB_0 \cdot r}{2m} \frac{y}{r} \\ v_{y,\text{in}} = v_{\phi,\text{in}} \cdot \cos\phi = \left(v_{\phi,\text{out}} - \frac{qB_0 \cdot r}{2m}\right) \cdot \cos\phi = v_{\phi,\text{out}} \sin\phi - \frac{qB_0 \cdot r}{2m} \frac{x}{r} \end{cases}$$

$$\begin{cases} v_{x,\text{in}} = v_{x,\text{out}} + \frac{qB_0 y}{2m} \\ v_{y,\text{in}} = v_{y,\text{out}} - \frac{qB_0 x}{2m} \end{cases}$$

If we now consider the kinetic energy conservation we find also the relation between the $v_{z,in}$ and the $v_{z,out}$:

$$\begin{aligned} &\frac{1}{2}mv_{x,\text{out}}^2 + \frac{1}{2}mv_{y,\text{out}}^2 + \frac{1}{2}mv_{z,\text{out}}^2 = \\ &\quad = \frac{1}{2}mv_{x,\text{in}}^2 + \frac{1}{2}mv_{y,\text{in}}^2 + \frac{1}{2}mv_{z,\text{in}}^2 \end{aligned} \tag{3.25}$$

so that

$$v_{z,\text{in}} = \sqrt{v_{x,\text{out}}^2 + v_{y,\text{out}}^2 + v_{z,\text{out}}^2 - v_{x,\text{in}}^2 - v_{y,\text{in}}^2}$$

Here's the map:

$$\begin{pmatrix} x_1 \\ y_1 \\ v_{x,1} \\ v_{y,1} \end{pmatrix} = \begin{pmatrix} 1 & 0 & 0 & 0 \\ 0 & 1 & 0 & 0 \\ 0 & \frac{qB_0}{2m} & 1 & 0 \\ -\frac{qB_0}{2m} & 0 & 0 & 1 \end{pmatrix} \cdot \begin{pmatrix} x_0 \\ y_0 \\ v_{x,0} \\ v_{y,0} \end{pmatrix}$$

while the map for the z was omitted because it's non-linear.

When the particle is coming out from the solenoid this is the map for the fringing field:

$$\begin{pmatrix} x_2 \\ y_2 \\ v_{x,2} \\ v_{y,2} \end{pmatrix} = \begin{pmatrix} 1 & 0 & 0 & 0 \\ 0 & 1 & 0 & 0 \\ 0 & -\frac{qB_0}{2m} & 1 & 0 \\ \frac{qB_0}{2m} & 0 & 0 & 1 \end{pmatrix} \cdot \begin{pmatrix} x_1 \\ y_1 \\ v_{x,1} \\ v_{y,1} \end{pmatrix}$$

3.5 Our simulations

In this paragraph I'll recap all the simulations that we have done for this transport problem.

3.5.1 Bunches from PIC simulations

First of all, we started using bunches obtained by Carlo Benedetti using ALaDyn code [39]. Those are *realistic* bunches, and because of this fact they were really hard to use when cross-checking results with other software (there's no way to understand at first sight some effects).

bunch3D v1

This is the original bunch. In fig. 3.5 there're the position distribution in x and y and in x and z, while in fig. 3.6 there're the energy distribution, obtained via β_z (in our code, the momenta are pure numbers, because they are divided by $m_p c$), and the transverse momentum distribution, β_x vs β_y.

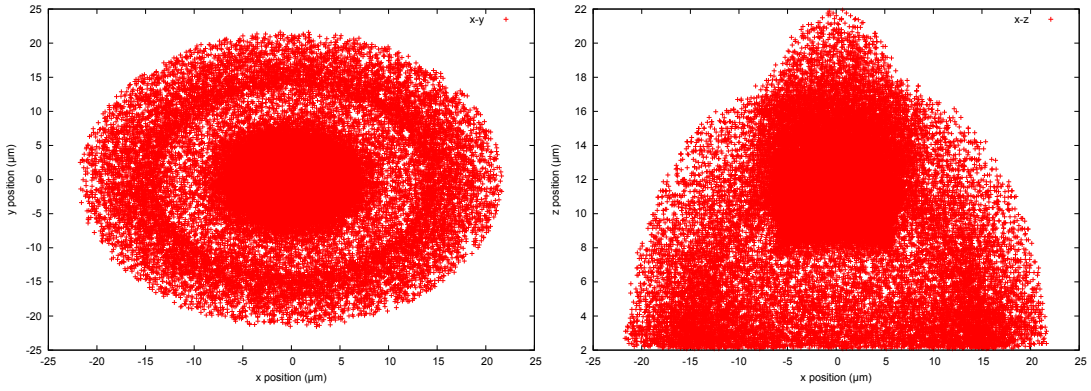

Figure 3.5: *bunch #1 particle distribution in xy (left) and xz (right)*

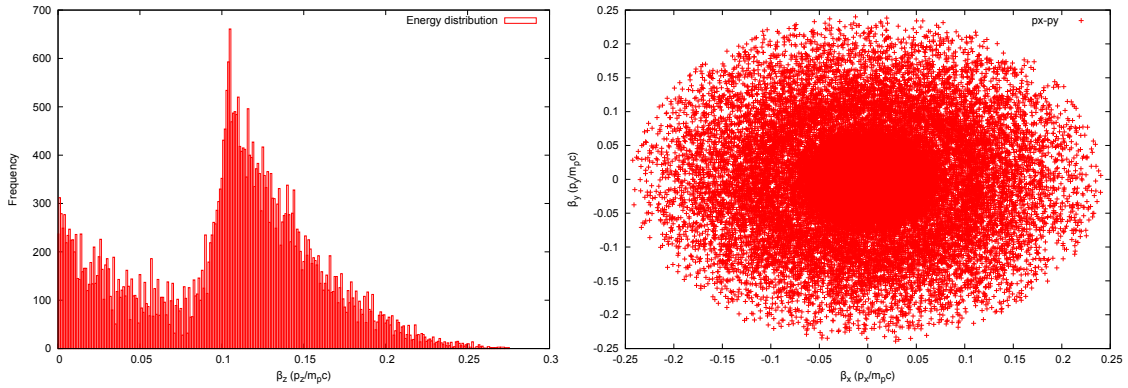

Figure 3.6: *bunch #1 energy distribution (β_z) (left) and transverse momentum distribution (β_x vs β_y) (right)*

bunch3D v2

This is the same bunch as before, but with some cuts applied, to make it more useful for our analysis. In figure 3.8 there're the energy distribution, obtained via β_z, and the transverse momentum distribution of the particles; in fig. 3.7 there're the position distribution in xy and xz.

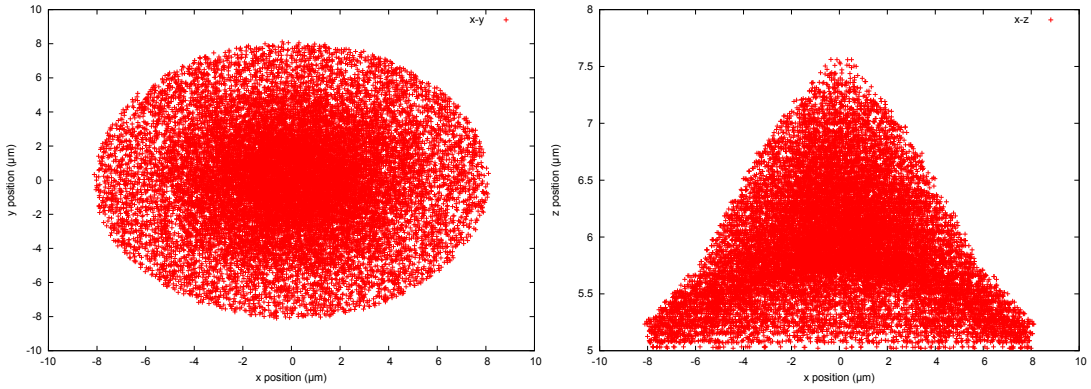

Figure 3.7: *bunch #2 particle distribution in xy and xz*

3.5.2 The typical beamlines analysed

FODO

First of all, our analysis was done on a classical quadrupole beamline, with a focusing quadrupole coupled with a defocusing one.

Characteristics of the beamline:

- focusing quadrupole length: 10 cm
- focusing quadrupole field gradient: 30 T/m
- defocusing quadrupole length: 10 cm
- defocusing quadrupole field gradient: 30 T/m

Results were not really very promising, because this beamline required very high gradients to keep emittance under control. As we can see from literature, in fact, quadrupoles with a so high gradient are still under investigations [40].

I+FODO+I

The analysis proceeded inserting two irises, at the beginning and at the end of the beamline, to further reduce the emittance. Unfortunately, with this choice, really very few protons survived!

Characteristics of the beamline:

- first iris radius: 0.5 mm
- second iris radius: 0.5 mm

Solenoid

Starting from my experience in Frankfurt, we began considering solenoids as effective focusing elements. We started with a really simple *hard edge* model of the solenoid, like those used for quadrupoles.

First of all we started with a configuration like Fig. 3.9. We immediately dropped both irises, because the losses were exaggerate.

After these simulations, we changed our transport beamline, simplifying with only an iris at the beginning and implementing more realistic models for the solenoid.

Characteristics of the beamline:

- initial drift of 1 cm
- solenoid length: 20 cm
- solenoid B-field: 30 T

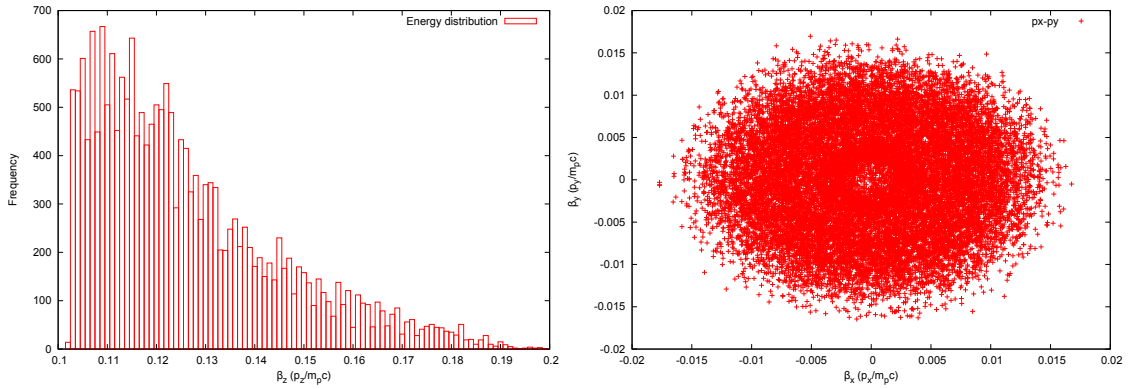

Figure 3.8: *bunch #2 energy distribution (β_z) (left) and transverse momentum distribution (β_x vs β_y) (right)*

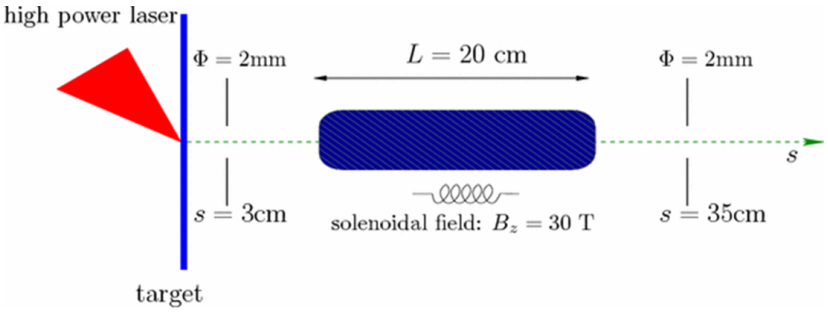

Figure 3.9: *Transport system model, as studied in this thesis.*

I+Solenoid

As just said, we tried also to further reduce emittances with an iris at the beginning of the solenoid.

Characteristics of the beamline:

- iris radius: 0.5 mm

Solenoid with fringing fields - Phelix beamline configuration

Describing the solenoids in a more realistic way was a key to the latest simulations. In Frankfurt I cross-checked our code with the kick-model at the beginning and at the end of the solenoid, using the parameters of the Phelix beamline from GSI.

- initial drift of 15 mm
- solenoid length: 72 mm
- solenoid B-field: 17.8 T (hard edge with kick model for fringing fields)

3.5.3 Status of the code at the end of the Frankfurt period

At the end of my period spent in Frankfurt dealing with those problem, our code dealt better with solenoids and passed checks against LORASR and Trace-3D codes. In the figure [3.10] I made a comparison between LORASR and PROPAGA and everything was really better. Also, we did some benchmarks with a custom-made bunch, with a 5 mm radius made of particles without transversal momentum, to see the differences between an hard edge model with and without the fringing fields treatment. As we can see from figure [3.11], the solenoid model without fringe fields is unable to focus this kind of bunches, while experimentally they're focused. It's a clear demonstration about the importance of these *corrections* in the simulations.

3.5.4 Simulations with K-V bunches

To better compare our code with ASTRA, LORASR and Trace 3-D, I also analysed many times my transport code with many different K-V distributed bunch and different beamlines. We can see some graphs in fig. 3.12, in which we can see how the bunch envelope is different for the same bunch when it's propagating into a beamline composed of only a solenoid at different B-field configurations.

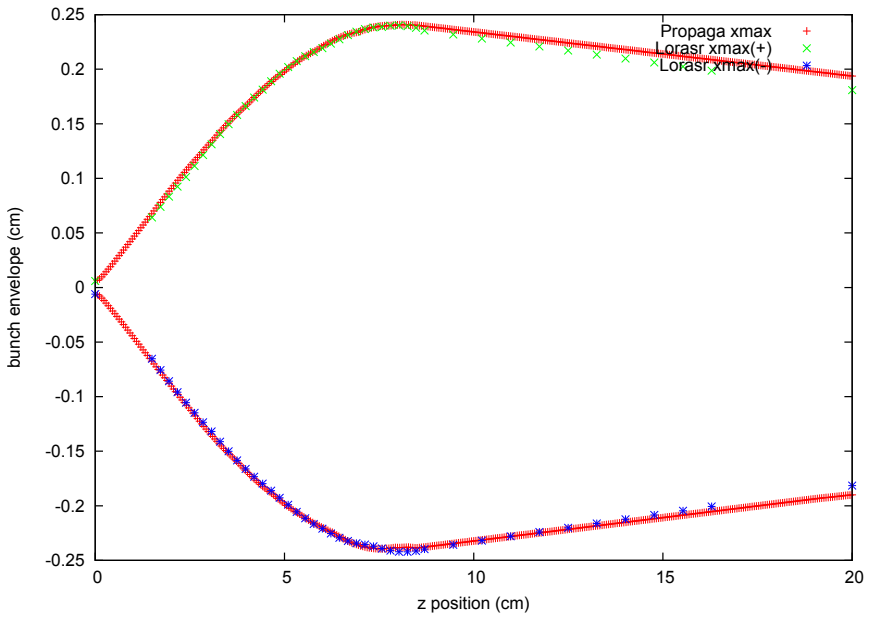

Figure 3.10: *bunch envelope (x along z) for a bunch with an energy of 10 MeV, a spread of 2% propagating in the Phelix beamline.*

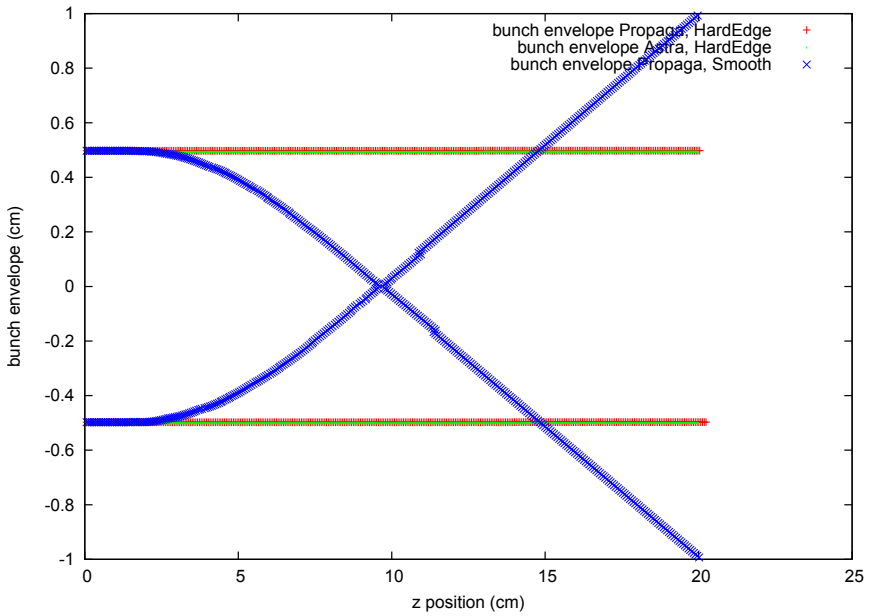

Figure 3.11: *bunch envelope (x along z) for a bunch without transversal momentum and an initial radius of 5 mm, in the Phelix beamline configuration.*

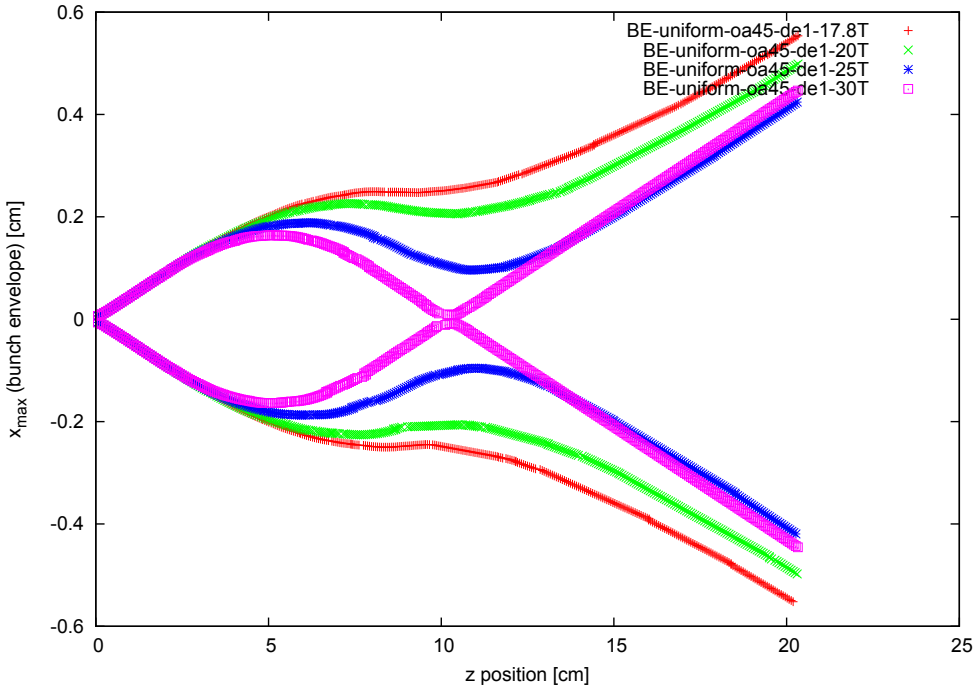

Figure 3.12: *bunch envelope for a uniform KV bunch with an energy spread of* 1% *and an opening angle* (x'/β_{zeta}) *of 45 mrad at different magnetic fields*

3.5.5 The hard edge approximation removed

Back in Italy, I worked on a much more realistic description of the field, to remove the hard edge approximation. Using a function designed to make a smoother Heaviside theta,

$$f(z, z_0, \lambda) = \frac{1}{\left(1 + e^{-(z-z_0)/\lambda}\right)} \tag{3.26}$$

which then gives a smoother delta:

$$f'(z, z_0, \lambda) = \frac{1}{\lambda} \frac{e^{-(z-z_0)/\lambda}}{\left(1 + e^{-(z-z_0)/\lambda}\right)^2} \tag{3.27}$$

we can now design a curve for the B-field that does not have any discontinuity. We can write the B field in this way:

$$\mathbf{B} = \begin{pmatrix} B_\rho \\ B_\phi \\ B_z \end{pmatrix} \tag{3.28}$$

so that the smoothed B_z is:

$$B_z = B_0 \left(f(z, 0, \lambda) - f(z, L_s, \lambda)\right) \tag{3.29}$$

From the divergence operator rewritten in cylindrical coordinates we get that

$$\nabla \cdot \mathbf{B} = \frac{1}{\rho}\partial_\rho \left(\rho B_\rho\right) + \frac{1}{\rho}\partial_\phi \left(B_\phi\right) + \partial_z B_z = 0 \tag{3.30}$$

so that we can write, after having imposed $B_\phi = 0$, a B_ρ like this:

$$B_\rho = -\frac{1}{2} B_0 \rho \left(f'(z, 0, \lambda) - f'(z, L_s, \lambda)\right) \tag{3.31}$$

so that

$$B_x = -\frac{1}{2} B_0 x \left(f'(z, 0, \lambda) - f'(z, L_s, \lambda)\right) \tag{3.32}$$

$$B_y = -\frac{1}{2} B_0 y \left(f'(z, 0, \lambda) - f'(z, L_s, \lambda)\right) \tag{3.33}$$

Doing the maths we get

$$\mathbf{F} = q \begin{pmatrix} B_z v_y + \frac{1}{2} v_z B_y \\ -B_z v_x - \frac{1}{2} v_z B_x \\ \frac{1}{2} B_x v_y - \frac{1}{2} B_y v_x \end{pmatrix} \tag{3.34}$$

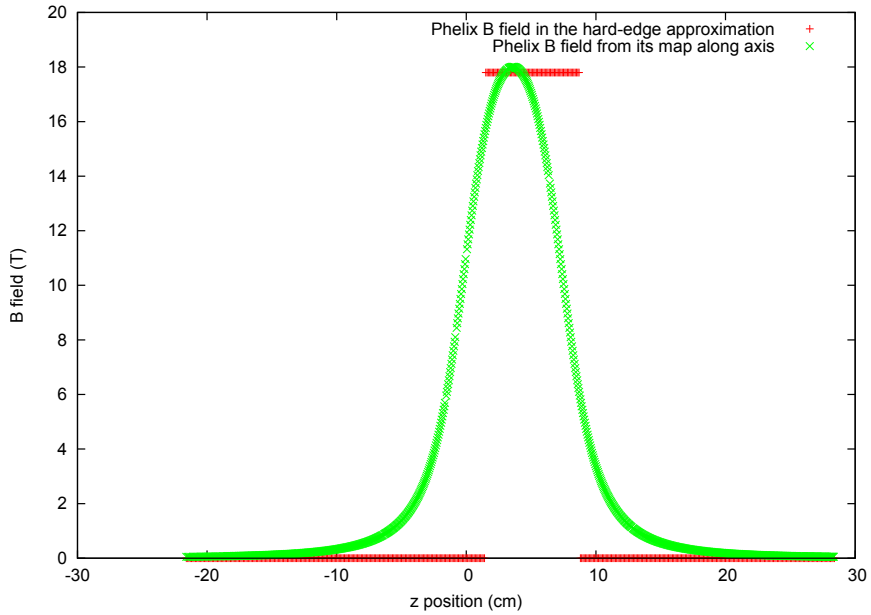

Figure 3.13: *B field comparison: the hard edge model and the smooth one.*

As we can see from the calculations above, dealing with a smooth B field brought also a realistic treatment of the fringing fields.

In figure 3.13 there are plotted the hard edge model of the Phelix B field and the more realistic one, which can be described analytically using the previous method.

In fig. 3.14 we can see the emittances along different beamlines for the transport of the bunch3D v2 obtained by Carlo Benedetti using the ALaDyn code to obtain a realistic bunch.

3.5.6 Future work

Propaga still lacks any proper treatment of space-charge effects and more realistic B-field treatment in all the elements except for the solenoid. Those will be the next tasks that will be done in the coming months. Analysing a recent article coming from a PHELIX Collaboration [41], they simulate both charged populations and their interactions. Due to their much lower energies, electrons that are co-moving with protons (have the same velocity as protons) get forced down to the solenoid axis directly at the target position, as can be seen from fig. 3.15 (the magnetic field at the target position is just about 0.95 T, enough to focus slow electrons). This effect has strong influence on proton propagation. The normally existing quasi neutrality of the beam is not preserved, there's a meaningful charge distribution. Hence, the protons get attracted by the negative space-charge of the electron beam, leading to a better focusing of the protons around the solenoid axis. This is a new

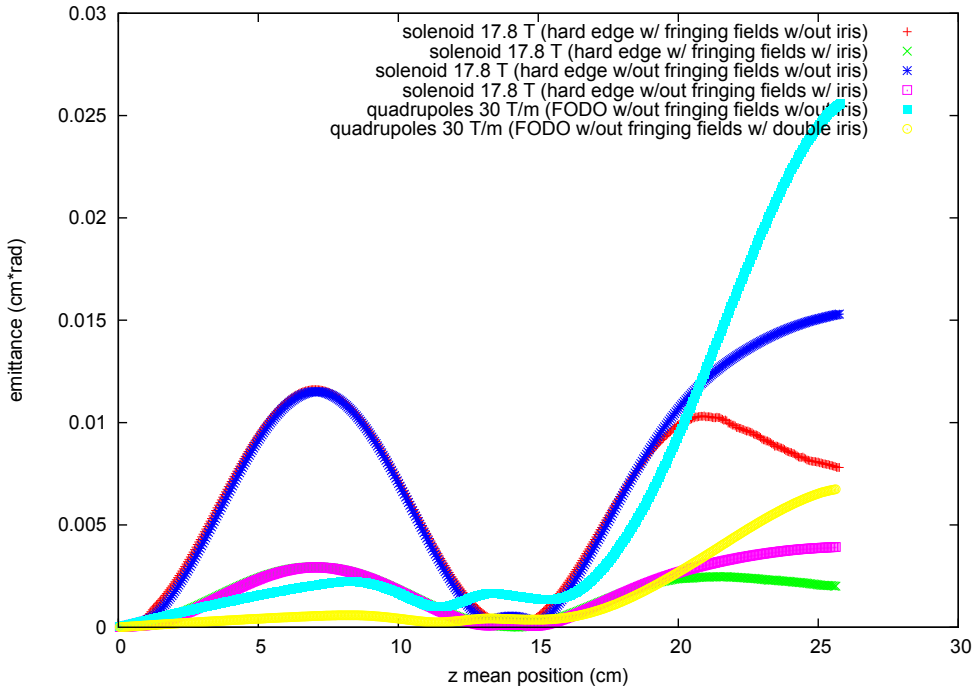

Figure 3.14: *emittance for the bunch3D v2 made by Carlo Benedetti*

and interesting effect that we did not even consider at the beginning of the work.

During my period of time spent at the Goethe University, I attended many really talks; in one of those, Prof. I. J. Petzenhauser from GSI talked about the magnetic horn as a device studied in recent years, useful to focus problematic bunches. But, as he said, works are done mainly on really high-energy particles [42] and so if we want to investigate it we would have to start from the beginning.

Leaving aside *Propaga*, also my bunch generator is still not checked when producing Gaussian bunches. I will need to check how it deals with them and maybe then we will use it for some new tests on *Propaga*. I found some people interested in it in Frankfurt, too.

Lastly, *Propaga* does not describe any type of post-acceleration, but we will need some code dealing with this problem to further analyse our desired beamline.

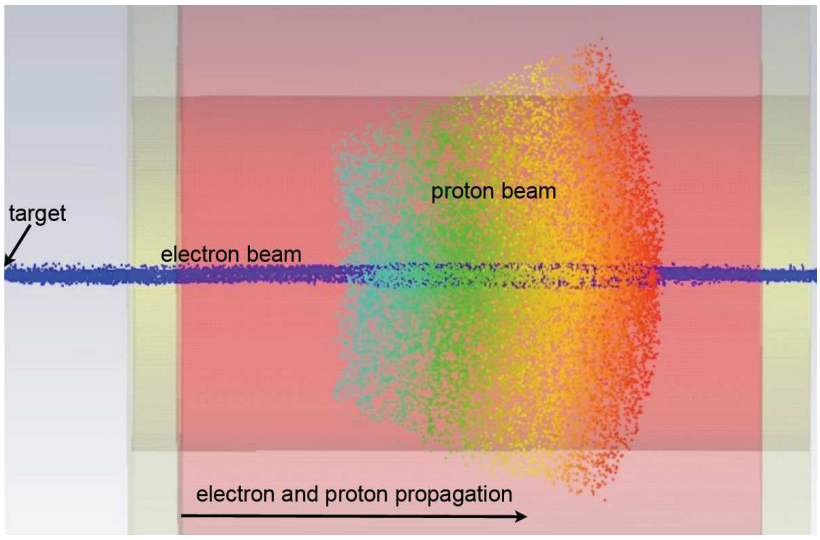

Figure 3.15: *Electron (blue) and proton (cyan to red) flux through the solenoid. The beam has entered the solenoid from the left side of the picture. The electrons are circulating around the axis of the solenoid, leading to a strong negative space charge that results in a proton beam focusing and aggregation around the axis too [41].*

Conclusion

In this thesis I described the work I did in the past year in the framework of the activities of the *Lilia-INFN* experiment at Bologna.

At the moment, here the main research field is the study of laser acceleration of protons. While electron acceleration is known relatively well, protons dynamic treatment, on the other hand, is still under investigation not only here but also in many other theoretical groups.

Significant experimental results were obtained only in last years, due to the dramatic improvements in laser power obtained with the chirped pulse amplification technique. Now, thanks also to the new kinds of targets, it seems that in the near future we will be capable of obtaining protons with energies above one hundred of MeV, sufficient for medical applications, such as hadron therapy.

In view of these future possibilities, the group is actively working to simulate the behaviour of innovative new targets, such as gaseous jet targets, and transport systems. The present work is also focused on the feasibility study of the Prometheus project that aims to create a laser based laboratory for the acceleration of protons for biomedical applications in collaboration with ENEA division of Bologna.

In the first chapter of this thesis I analysed the main features of laser-plasma acceleration and the two main laser-proton acceleration regimes. For both of them I described their distinctive features and the energies achievable with current technology. These regimes are studied and simulated here in Bologna with ALaDyn, a particle-in-cell code developed by the Bologna's group itself. My contribution to ALaDyn was the development of algorithms and associated code to integrate the particle equations of motions using leapfrog and symplectic methods.

In the third chapter I described the main work of my thesis: I studied the problems of transport of the protons bunches, obtained from laser-plasma interactions. The main concern was to limit the growth of emittance with suitable arrangement of focusing devices. This is a key point to couple these bunches with a post-acceleration devices which might be used for cancer treatment.

The first studies on transport system concerned a FODO beamline (focusing-defocusing coupled quadrupoles). To improve my knowledge on this topic I spent a period of two months at the Goethe University in Frankfurt am Main where I collaborated with Prof. Ratzinger's group. Their main activity is the design of new cavities for post-acceleration. There I learnt the importance of solenoids as focusing devices in a beamline; the model we had initially considered did not include the fringing fields of the solenoid itself. After inserting them, a good agreement with results obtained by the Frankfurt group were obtained.

I also wrote a bunch generator, to simulate a K-V beam, whose propagation was used to match with their results. Other simulations were based on bunches obtained from the PIC code ALaDyn.

The results presented here are preliminary even though they show that a laser accelerated bunch can be transported with a controlled emittance growth. For the future, we plan to insert the space charge forces and to add the electronic population in our simulations which has a focusing effect on protons. A crucial point will be the consideration of different types of targets which allow to obtain a better bunch for transport.

Stefano Sinigardi
stefano.sinigardi@gmail.com

Bibliography

[1] R.J. Goldston and P.H. Rutherford. *Introduction to Plasma Physics*. Introduction to Plasma Physics. Taylor & Francis, 2010.

[2] C. Joshi. Plasma Accelerators. *Scientific American*, 294(2):020000–47, February 2006.

[3] Gerard A. Mourou, Toshiki Tajima, and Sergei V. Bulanov. Optics in the relativistic regime. *Rev. Mod. Phys.*, 78:309–371, Apr 2006.

[4] A. Sgattoni. Equazioni di Maxwell-Liouville ed accelerazione di cariche tramite un impulso elettromagnetico. Master's thesis, University of Bologna, 2005–2006.

[5] Gérard A. Mourou and Donald Umstadter. Extreme light. *Scientific American*, page 81, May 2002.

[6] W. P. Leemans, B. Nagler, A. J. Gonsalves, C. Tóth, K. Nakamura, C. G. R. Geddes, E. Esarey, C. B. Schroeder, and S. M. Hooker. GeV electron beams from a centimetre-scale accelerator. *Nature Physics*, 2:696–699, October 2006.

[7] W.L. Kruer. *The Physics of Laser Plasma Interactions*. Frontiers in physics. Westview Press, 2003.

[8] G. Turchetti, A. Sgattoni, C. Benedetti, P. Londrillo, and L. Di Lucchio. Comparison of scaling laws with {PIC} simulations for proton acceleration with long wavelength pulses. *Nuclear Instruments and Methods in Physics Research Section A: Accelerators, Spectrometers, Detectors and Associated Equipment*, 620(1):51 – 55, 2010. COULOMB09 Ions Acceleration with high Power Lasers: Physics and Applications.

[9] Andrea Macchi, Silvia Veghini, and Francesco Pegoraro. "Light Sail" acceleration reexamined. *Phys. Rev. Lett.*, 103:085003, Aug 2009.

[10] C. A. J. Palmer, N. P. Dover, I. Pogorelsky, M. Babzien, G. I. Dudnikova, M. Ispiriyan, M. N. Polyanskiy, J. Schreiber, P. Shkolnikov, V. Yakimenko, and Z. Najmudin. Monoenergetic Proton Beams Accelerated by a Radiation Pressure Driven Shock. *Physical Review Letters*, 106(1):014801, January 2011.

[11] Andrea Macchi, Federica Cattani, Tatiana V. Liseykina, and Fulvio Cornolti. Laser acceleration of ion bunches at the front surface of overdense plasmas. *Phys. Rev. Lett.*, 94:165003, Apr 2005.

[12] M. Passoni and M. Lontano. One-dimensional model of the electrostatic ion acceleration in the ultraintense laser-solid interaction. *Laser and Particle Beams*, 22(02):163–169, 2004.

[13] V. T. Tikhonchuk. Interaction of a beam of fast electrons with solids. *Physics of Plasmas (1994-present)*, 9(4):1416–1421, 2002.

[14] Alessandro Zani, Andrea Sgattoni, and Matteo Passoni. Parametric investigations of target normal sheath acceleration experiments. *Nuclear Instruments and Methods in Physics Research Section A: Accelerators, Spectrometers, Detectors and Associated Equipment*, 653(1):94 – 97, 2011. Superstrong 2010.

[15] T. Esirkepov, M. Yamagiwa, and T. Tajima. Laser ion-acceleration scaling laws seen in multiparametric particle-in-cell simulations. *Phys. Rev. Lett.*, 96:105001, Mar 2006.

[16] T. Esirkepov, M. Borghesi, S. V. Bulanov, G. Mourou, and T. Tajima. Highly efficient relativistic-ion generation in the laser-piston regime. *Phys. Rev. Lett.*, 92:175003, Apr 2004.

[17] Andrea Macchi, Tatiana V. Liseikina, Sara Tuveri, and Silvia Veghini. Theory and simulation of ion acceleration with circularly polarized laser pulses. *Comptes Rendus Physique*, 10(2–3):207 – 215, 2009. Laser acceleration of particles in plasma - Accélération laser de particules dans les plasmas.

[18] Andrea Macchi and Carlo Benedetti. Ion acceleration by radiation pressure in thin and thick targets. *Nuclear Instruments and Methods in Physics Research Section A: Accelerators, Spectrometers, Detectors and Associated Equipment*, 620(1):41 – 45, 2010. Coulomb'09 - Ions Acceleration with high Power Lasers: Physics and Applications.

[19] F. Cattani, A. Kim, D. Anderson, and M. Lisak. Threshold of induced transparency in the relativistic interaction of an electromagnetic wave with overdense plasmas. *Phys. Rev. E*, 62:1234–1237, Jul 2000.

[20] A P L Robinson, P Gibbon, M Zepf, S Kar, R G Evans, and C Bellei. Relativistically correct hole-boring and ion acceleration by circularly polarized laser pulses. *Plasma Physics and Controlled Fusion*, 51(2):024004, 2009.

[21] A P L Robinson, M Zepf, S Kar, R G Evans, and C Bellei. Radiation pressure acceleration of thin foils with circularly polarized laser pulses. *New Journal of Physics*, 10(1):013021, 2008.

[22] T. Schlegel, N. Naumova, V. T. Tikhonchuk, C. Labaune, I. V. Sokolov, and G. Mourou. Relativistic laser piston model: Ponderomotive ion acceleration in dense plasmas using ultraintense laser pulses. *Physics of Plasmas (1994-present)*, 16(8), 2009.

[23] G. Turchetti. *Dinamica classica dei sistemi fisici.* Collana di fisica. Testi e manuali. Zanichelli, 1998.

[24] C.K. Birdsall and A.B. Langdon. *Plasma Physics via Computer Simulation.* Series in Plasma Physics. Taylor & Francis, 2004.

[25] M. Schollmeier, S. Becker, M. Geißel, K. A. Flippo, A. Blažević, S. A. Gaillard, D. C. Gautier, F. Grüner, K. Harres, M. Kimmel, F. Nürnberg, P. Rambo, U. Schramm, J. Schreiber, J. Schütrumpf, J. Schwarz, N. A. Tahir, B. Atherton, D. Hab, B. M. Hegelich, and M. Roth. Controlled transport and focusing of laser-accelerated protons with miniature magnetic devices. *Phys. Rev. Lett.*, 101:055004, Aug 2008.

[26] P Antici, J Fuchs, E d'Humières, J Robiche, E Brambrink, S Atzeni, A Schiavi, Y Sentoku, P Audebert, and H Pépin. Laser acceleration of high-energy protons in variable density plasmas. *New Journal of Physics*, 11(2):023038, 2009.

[27] K. Zeil, S. D. Kraft, S. Bock, M. Bussmann, T. E. Cowan, T. Kluge, J. Metzkes, T. Richter, R. Sauerbrey, and U. Schramm. The scaling of proton energies in ultrashort pulse laser plasma acceleration. *New Journal of Physics*, 12(4):045015, 2010.

[28] INFN Collaboration. SL-LILIA INFN project. `http://sl-lilia.mi.infn.it`.

[29] R. Tiede, G. Clemente, H. Podlech, U. Ratzinger, A.C. Sauer, et al. LORASR code development. *Conf.Proc.*, C060626:2194–2196, 2006.

[30] D. P. Rusthoi, W.P. Lysenko, and K. R. Crandall. Further improvements in trace 3-d. In *Particle Accelerator Conference, 1997. Proceedings of the 1997*, volume 2, pages 2574–2576 vol.2, May 1997.

[31] I.M. Kapchinskij and V.V. and Vladimirskij. Limitations Of Proton Beam Current In A Strong Focusing Linear Accelerator Associated With The Beam Space Charge. pages 274–287, 1959.

[32] A. Vivoli, C. Benedetti, and G. Turchetti. Time series analysis of coulomb collisions in a beam dynamics simulation. *Nuclear Instruments and Methods in Physics Research Section A: Accelerators, Spectrometers, Detectors and Associated Equipment*, 561(2):320 – 324, 2006. Proceedings of the Workshop on High Intensity Beam Dynamics Coulomb05 Workshop on High Intensity Beam Dynamics.

[33] K. Flöttmann. ASTRA. `http://www.desy.de/~mpyflo`, 2000.

[34] K. Flöttmann, S. M. Lidia, and P. Piot. Recent improvements to the ASTRA particle tracking code. In *Proceedings of PAC03*, pages 3500–3502, 2003.

[35] Ali Almomani, Martin Droba, Ulrich Ratzinger, and Ingo Hofmann. Matching the Laser Generated p-bunch into a CH-DTL. *Conf.Proc.*, C100523:THPD035, 2010.

[36] Armando Bazzani, Graziano Servizi, Ezio Todesco, and Giorgio Turchetti. *A normal form approach to the theory of nonlinear betatronic motion*. CERN, Geneva, 1994.

[37] H. Wiedemann. *Particle Accelerator Physics*. Advanced Texts in Physics. Springer, 2003.

[38] G. Franchetti. Linear beam optics in solenoidal channels. *Phys. Rev. ST Accel. Beams*, 4:074001, Jul 2001.

[39] C. Benedetti, A. Sgattoni, G. Turchetti, and P. Londrillo. ALaDyn: A high-accuracy PIC code for the Maxwell-Vlasov equations. *IEEE Transactions on Plasma Science*, 36(4):1790 –1798, aug. 2008.

[40] E. Fischer, G. Moritz, N.N. Agapov, V. Bartenev, A. Donyagin, et al. Design and Study of a Superferric Model Dipole and Quadrupole Magnets for the GSI Fast-pulsed Synchrotron SIS100. 2004.

[41] K. Harres, I. Alber, A. Tauschwitz, V. Bagnoud, H. Daido, M. Gunther, F. Nurnberg, A. Otten, M. Schollmeier, J. Schutrumpf, M. Tampo, and M. Roth. Beam collimation and transport of quasineutral laser-accelerated protons by a solenoid field. *Physics of Plasmas*, 17(2):023107, 2010.

[42] S Gilardoni, G Grawer, G Maire, J M Maugain, S Rangod, and F Voelker. Status of a magnetic horn for a neutrino factory. *Journal of Physics G: Nuclear and Particle Physics*, 29(8):1801, 2003.